공학박사 학위논문

Near-eye displays with wide field of view using anisotropic optical elements

비등방성 광학 소자를 이용한

광 시야각 근안 디스플레이

2019년 2월

서울대학교 대학원

전기·컴퓨터공학부

홍 종 영

Near-eye displays with wide field of view using anisotropic optical elements

지도 교수 이 병 호

이 논문을 공학박사 학위논문으로 제출함

2019년 2월

서울대학교 대학원

전기·컴퓨터공학부

홍 종 영

홍종영의 공학박사 학위논문을 인준함

2019년 2월

위 원 장 _____

부위원장 _____

위 원 _____

위 원 _____

위 원 _____

Abstract

Near-eye displays with wide field of view using anisotropic optical elements

Jong-Young Hong

Department of Electrical Engineering and Computer Science

College of Engineering

Seoul National University

Near-eye display is considered as a promising display technique to realize augmented reality by virtue of its high sense of immersion and user-friendly interface. Among the important performances of near-eye display, a field of view is the most crucial factor for providing a seamless and immersive experience for augmented reality. In this dissertation, a transmissive eyepiece is devised instead of a conventional reflective eyepiece and it is discussed how to widen the field of view without loss of additional system performance. In order to realize the transmissive eyepiece, the eyepiece should operate lens to virtual information and glass to real-world scene. Polarization multiplexing technique is used to implement the multi-functional optical element, and anisotropic optical elements are used as material for multi-functional optical element.

To demonstrate the proposed idea, an index-matched anisotropic crystal lens has been presented that reacts differently depending on polarization. With the combination of isotropic material and anisotropic crystal, the index-

matched anisotropic crystal lens can be the transmissive eyepiece and achieve the large field of view.

Despite the large field of view by the index-matched anisotropic crystal lens, many problems including form factor still remain to be solved. In order to overcome the limitations of conventional optics, a metasurface is adopted to the augmented reality application. With a stunning optical performance of the metasurface, a see-through metasurface lens is proposed and designed for implementing wide field of view near-eye display.

The proposed novel eyepieces are expected to be an initiative study not only improving the specification of the existing near-eye display but opening the way for a next generation near-eye display.

Keywords: Near-eye display, augmented reality, mixed reality, anisotropic crystal, metasurface, metasurface lens, holographic display, light field display
Student Number: 2013-20910

Contents

List of Table

List of Figures

Chapter 1 Introduction

1.1 Near-eye displays for augmented reality

Augmented reality (AR) refers to enhanced reality by superimposing computer generated information across the human senses including visual, auditory and haptic sense. It is often compatible with mixed reality or computer mediated reality according to the dominance of virtuality and mediality [1].

Among the various senses, the most important stimuli for AR perception is visual stimuli [1, 2], so there have been lots of display techniques to realize AR. From the stereoscopic display, autostereoscopic display and now to handheld mobile AR devices, various techniques have taken the path to realize AR [3-12]. However, erstwhile displays suffer from difficulties in reducing heterogeneity between virtual information and the real-world owing to narrow field of view (FOV), bulky form factor and low resolution.

For providing realistic virtual information, a near-eye display has been actively studied for special purposes such as martial use and medical uses in the past few decades [11]. The near-eye display provides three-dimensional (3D) information to both eyes with a spectacle. The difference between the near-eye display and the conventional stereoscopic display is the position of the display. In the stereoscopic display, the display is located in distant and polarized- or shutter glasses are used to display different images to the two

eyes [13]. On the other hands, the near-eye display uses two displays located right in front of each eye and displays the image into the both eyes. Thus, it is the feature of the near-eye display to use an eyepiece for floating the image to the desired depth.

However, the erstwhile near-eye display is inappropriate to be used as a display for realizing AR due to the structural limitations of the display itself. Especially, the eyepiece and opaque display located in front of the eye distort the information of the real-world scene. Thus, a structure that does not distort the real-world scene should be devised while succeeding the various advantages of the near-eye display. In addition, since near-eye display for AR requires interaction with various reactions in the real-world, the device itself should be mixed into reality. In other words, every technical problem such as compact form factor, interaction technique, battery problems, and calculation load, should be solved to be a socially acceptable device. Therefore, there have been a lot of challenges to realize the near-eye display for AR.

1.2 Optical performances of near-eye display

Ideal near-eye display for AR requires a high resolution and a wide FOV for reducing the sense of heterogeneity with the real-world, and it should provide a focus cue for natural overlap with real objects. In addition, a compact and lightweight form factor is essential for the user to wear over a duration of time, and a wide eyebox should be formed robustly for pupil sweeping. However, all these performances are in full of trade-off relation, and one is increased by sacrificing the other performance. For example, there

are ways to sacrifice the form factor to obtain the wide FOV, or to obtain the wide eyebox by reducing the FOV. Therefore, it is necessary to accurately evaluate performance of near-eye displays and devise a way to improve the performance without sacrificing other ones.

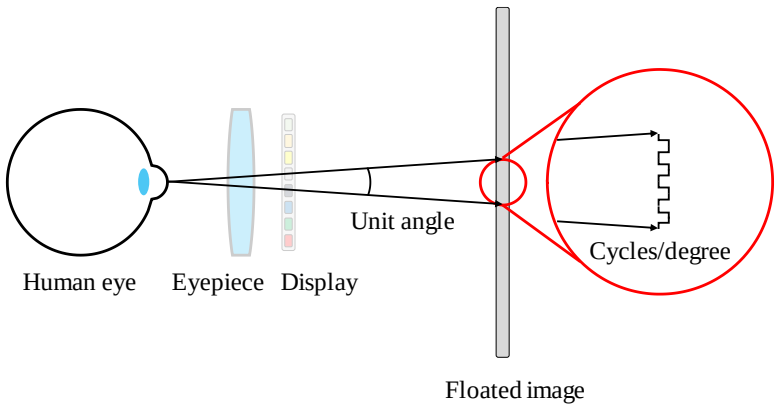

Figure 1.1 Resolution of the near-eye display.

As shown in Fig. 1.1, the resolution can be defined as the number of pixels per unit angle whose unit is cycles per degree (cpd). Since the human eye theoretically has a fine maximum resolution of 30 to 50 cpd, the resolution of the panel should be increased within this limitation [14]. In a practical situation, a near-eye display with a FOV of 60 degrees would have horizontal resolution of 16 cpd with 1920 pixels (FHD) but a near-eye display with a FOV of 90 degrees with same panel would only provide about 11 cpd. Thus, the resolution of the near-eye display is closely related to the FOV of the system and the resolution of the panel.

However, no matter how high-resolution panels are used, there is a limitation of the image quality due to the aberration and diffraction limit of

the optical system. Therefore, the modulation transfer function, which considers the contrast and frequency, would be used as an indicator of the resolution of the display.

To increase the resolution of near-eye display, there are two ways: a method of increasing the amount of information such as time multiplexing and a method of efficiently distributing information. Especially, the method of efficiently distributing a limited amount of information is called foveated rendering [15, 16]. The foveated rendering distributes the pixels of display in accordance with the distribution of a human optic nerve by projecting more information to the paracentral area and less information to the peripheral area.

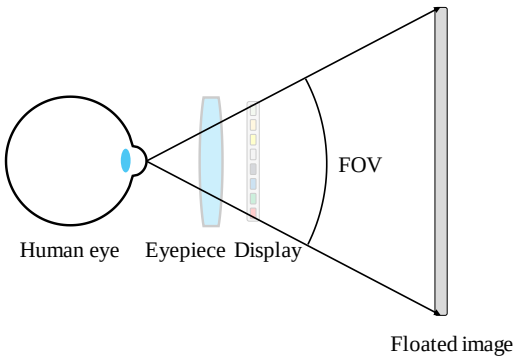

(a)

AR view from narrow FOV AR view from wide FOV

(b)

Figure 1.2 FOV of the near-eye display: (a) illustration of FOV and (b) AR view according to the FOV.

Field of view is one of the most important parts for immersive AR realization. There are various definitions of FOV in near-eye display, but in this dissertation, the FOV is defined by the angle between the floated image and an eye as shown in Fig. 1.2(a). Figure 1.2(b) shows the effect of FOV for AR view. Human visual system has about FOV of 160° for an eye [17]. Thus, it is extremely difficult to cover full FOV of human eye, so the minimum criterion for immersive near-eye display has been studied [18]. In general, the minimum FOV of near-eye display for immersive virtual reality is about 80 degrees where the stereo window is vanished. The stereo window is the boundary of the floated images corresponding to the left eye and right eye in the near-eye display. If the boundary is observed, the sense of immersion is deteriorated. Therefore, it is necessary to provide the FOV of 80° or more in order to realize the immersive near-eye display.

However, the FOV is also on the trade-off relation with various optical performances. For example, there is a near-eye display with wide FOV over 90° using bulky optical elements while a near-eye display with compact form factor of a few millimeters has FOV of less than 40°.

Since the FOV is the most essential performance for realizing AR through near-eye display, various attempts have been made to enlarge the FOV. Especially, it has been studied to break the trade-off relation between FOV and other ones with the development of eyepiece and display techniques.

(a)

Without focus cue With focus cue

(b)

Figure 1.3 Focus cue in near-eye display: (a) blur effect with focus cue and (b) comparison between with and without focus cue.

Figure 1.3(a) shows the importance of the focus cue in realizing AR. The depth of field of human eye is about 0.6 diopter (D), objects or images at different depths are blurred differently [19]. Therefore, the virtual information should be blurred differently depending on its depth information. However, without focus cue in near-eye display, virtual image is floated on fixed plane, so it hinders the virtual information to be overlapped with real-world objects located in various depth as shown in Fig. 1.3(b). Besides the affection of focus cue for sense of immersion, availability of giving focus cue in near-eye display is related to an eye fatigue [20, 21]. There are four physiological cues for human to perceive the depth, and it is widely known that the accommodation and the convergence do not match in a conventional

3D display. These accommodation-vergence conflict has been considered as a cause of eye fatigue and various methods have been proposed to mitigate it. Especially, in near-eye display, it is more important to give the focus cue on the display because the accommodation-vergence conflict can cause more severe eye fatigue because virtual information should cover a wide range of depth.

Therefore, the near-eye display uses various methods such as a super multi-view, a layered display, and a scanning method which gives focus cue in existing 3D display. In addition, a holographic near-eye display capable of providing a full wavefront gives complete focus cue, so it is considered as the next move of the near-eye display despite various obstacles in holographic display.

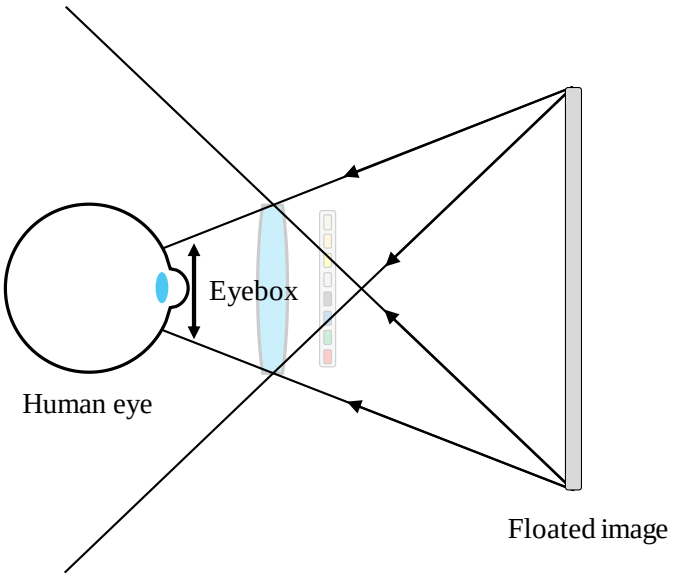

Figure 1.4 Eyebox of the near-eye display.

An eyebox is an area where an intact image can be observed within the radiance of the light formed with the near-eye display as shown in Fig. 1.4. A wide eyebox provides a comfortable AR experience regardless of the interocular distance. Thus, it is ideal to provide an eyebox of about 15 mm or more, but it is quite difficult to constitute such a wide eyebox. Therefore, many applications build an eyebox similar to the size of the pupil wherein the user manually adjusts the near-eye display for interocular distance [22]. Moreover, some systems even use dynamic pupil tracking system for pupil swim [23].

The eyebox is closely related to FOV. When the pupil swims within the eyebox, the FOV corresponding to the eyebox is defined as the common area of the image across the eyebox. Thus, if the size of the common area reduces, the size of the eyebox increases while the FOV decreases. Conversely, if the size of the image increases, the eyebox reduces while the FOV is increased. The relationship between these two parameters is known as an etendue. The etendue is suitable for comparing the FOV and the eyebox of various systems because it represents light spread in area and angle. In general, since the etendue is conserved in an optical system, it effectively describes the relation between the FOV and the eyebox.

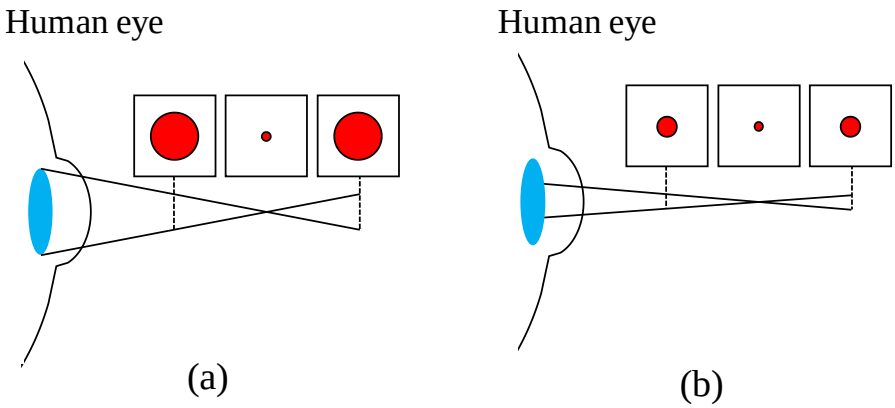

Figure 1.5 Effect of the eyebox on focus cue: (a) large eyebox and (b) small eyebox.

Besides the etendue between the FOV and the eyebox, the eyebox is also closely related to the focus cue. The focus cue is related with how fine the depth can be expressed with the display. Since the depth of field is inversely related to the size of the aperture, the size of light entering the human eye through the eyebox decides the focus cue. In other words, the large eyebox causes a fine depth resolution and also gives strong focus cues and vice versa as shown in Figs. 1.5(a) and (b).

The eyebox is an important parameter that not only provides a user with a comfortable AR viewing environment but is also closely related to the optical performance of virtual information such as the focus cue and the FOV.

It is important to set each parameter appropriately for the purpose of a near-eye display because parameters are in the full trade-off relation. Therefore, it is necessary to study the innovative near-eye display structure

for overcoming this trade-off relation.

1.3 State-of-the-arts of near-eye display

From the Wheatstone's stereoscope, head-mounted display (HMD) has been constantly developed for many different purposes such as medical use, martial use and educational use [11]. Derived from a simple toy with two still pictures, the era of lightweight and compact stand-alone HMD has finally arrived [22, 24-26]. Attempts have been made to provide wide FOV and natural 3D images after first HMD products have failed to commercialize due to the shortcomings of narrow FOV and inconvenient user interfaces. In order to overcome these drawbacks, the next wave of commercialization comes with the development of near-eye display technology, user-friendly interface and interactive features [22, 26]. However, the form factor and the wide FOV still have room for improvement.

The optical building blocks of the near-eye display are divided into three parts: an eyepiece, an optical combiner and a display part. The eyepiece is an optic that allows a display panel located near the eye to be well augmented with the real-world scene. The optical combiner combines virtual information from the display with the real-world scene and relays it to the eyepiece.

Also, various display techniques are adopted to the HMD such as simple 2D panel, projection and even holography. These three optical building blocks of the near-eye display are tightly connected to one another and should be combined properly in order to maximize the optical

performance.

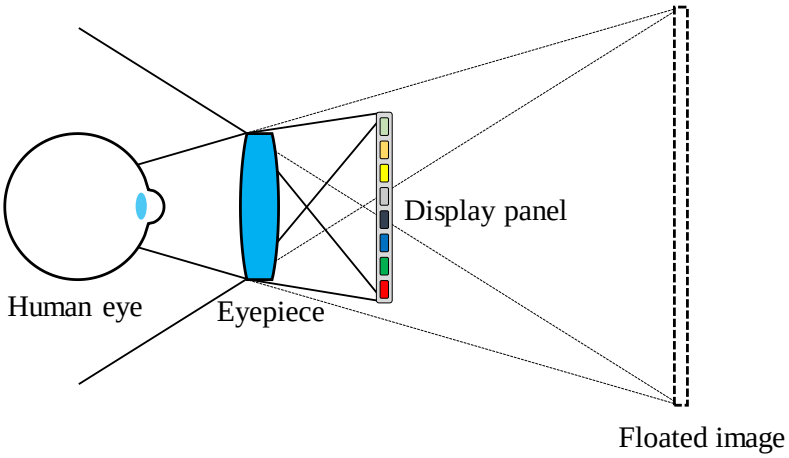

Figure 1.6 Configuration of conventional near-eye display for virtual reality.

The conventional near-eye display for virtual reality uses a convex lens as the eyepiece to float the display to a desired depth as shown in Fig. 1.6. However, as described above, this structure is not suitable for use in realizing AR due to the opaque display and the convex lens. In order to resolve said problems, most systems place the display on the side of the system to solve this problem and employ a see-through optical combiner, which combines the display on the side and the real-world scene.

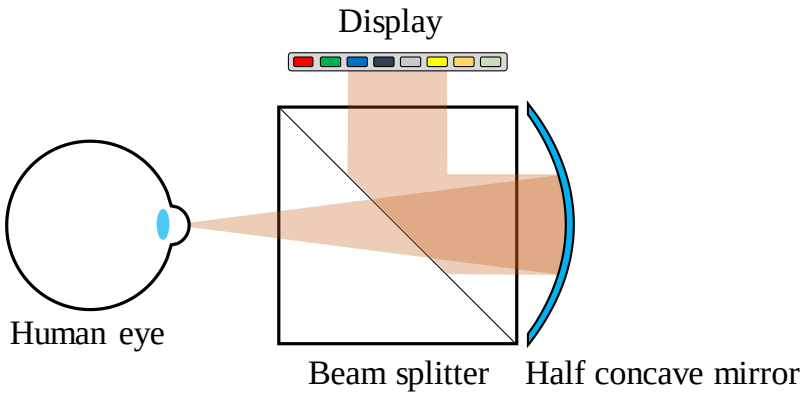

Figure 1.7 Principle of the bird bath type near-eye display.

The most prominent method is the bird bath system using a half concave mirror and a beam splitter as shown in Fig. 1.7. The display is located on the side of the system and the beam splitter transparently combines the display and the real-world scene. The half concave mirror is used for transparent eyepiece that functions a thin slab structure to the light from real-world while a concave mirror to the virtual information.

Because of its simple structure and robust system characteristics, the bird bath system is adopted in many commercial systems [27-30]. Moreover, the bird bath system has the advantage of providing relatively wide FOV and eyebox. However, since the beam splitter is used as the optical combiner, it is difficult to implement compact system. To solve these drawbacks, various methods such as using off-axis half concave mirror or free form optic have been devised, but due to the aberrations problem and the difficulty in fabrication, there still is no clear solution in using the bird bath system [29, 30].

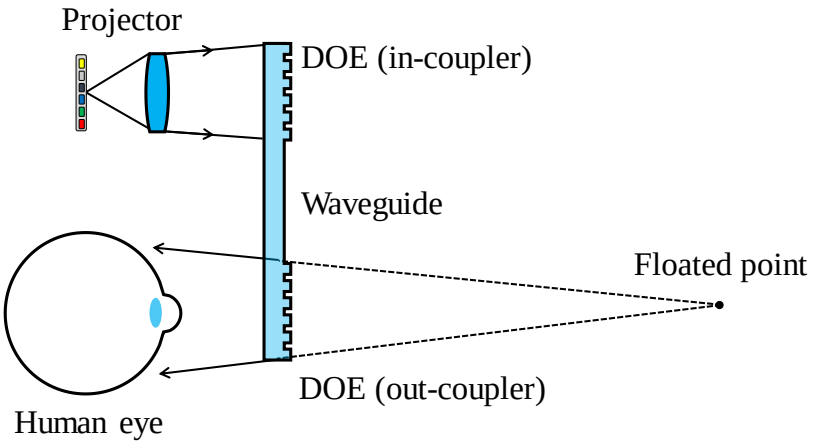

Figure 1.8 Principle of the near-eye display using diffractive optical elements and waveguide.

Recently, a combination using diffractive optical elements (DOEs) and waveguide has been proposed for realizing a compact near-eye display [22, 31, 32]. The basic configuration of near-eye display using DOEs and waveguide is shown in Fig. 1.8. The light from the projector has different directions for each pixel by an in-coupled DOE and the directionality is preserved by the waveguide. The transmitted virtual information is reproduced by an out-coupled DOE. Due to the beam expanding effect of DOEs, the system is equipped with a wide eyebox and a highly compact form factor of few millimeters. Despite great advantages, the total internal reflection condition of the waveguide limits the FOV to less than 40°, and the chromatic aberration of DOEs render it difficult to actually implement. Thus, it is still premature to say that this is the ultimate solution to the near-eye display.

Studies using holographic optical element (HOE) have been recently reported as a kind of next-generation near-eye display [33-35]. A volume grating is recorded for implementing HOE by interfering the wavefront of desired optical elements and reference wave on the photoreactive medium. Due to high transparency and thinness of photopolymers mainly used as the photoreactive medium, HOE is highly applicable as the eyepiece for near-eye display. Along with the fine medium properties, it is advantageous in improving various performance of the near-eye.

However, despite these advantages, since the photopolymer is vulnerable to humidity and temperature, and also has a non-uniform medium characteristic depending on the recording environment, further development on the material properties is required.

There are various display techniques for the near-eye display. A 2D panel is floated to a distance so that the 3D image can be perceived by the binocular disparity. This is a simple and effective way of minimizing the computational load and optical bulkiness, but it fails to provide the accommodation cue, or the focus cue, which can lead to eye fatigue when worn for a duration of time. Moreover, without the focus effect, virtual information fails to seamlessly overlap with the real-world scene.

Therefore, in order to provide focus cue, various display techniques including light field display, retinal direction projection, and holography have been adopted to the near-eye display.

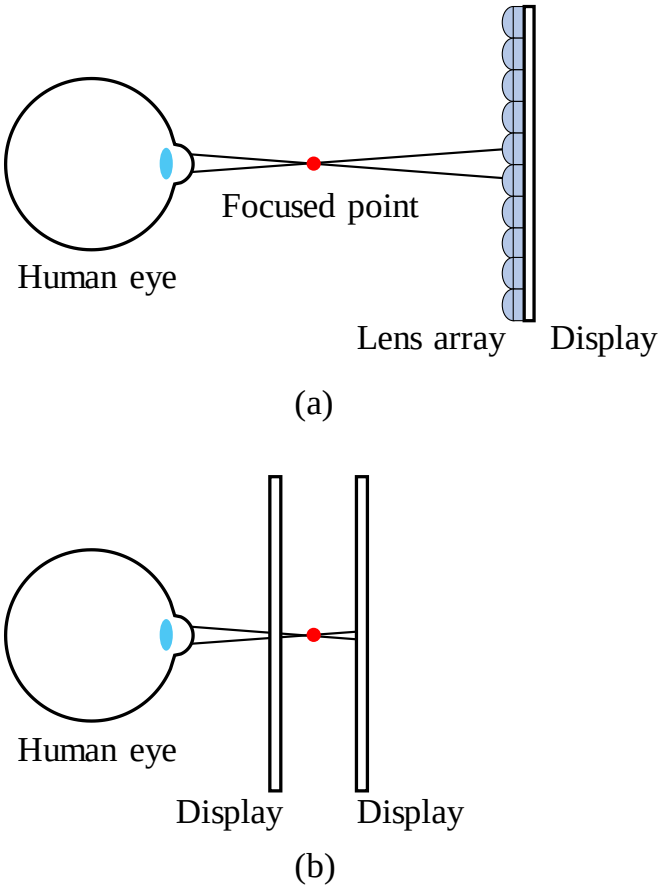

Figure 1.9 Principle of the light field display: (a) lenticular lens display and (b) multi-layered display.

Figure 1.9 depicts how the light field display makes a point in the air. The representative light field display, mainly used in near-eye displays, is integral imaging and layered display. In lenticular lens display, focus cue can be provided in a super-multi-view condition where two or more viewpoints enter the pupil simultaneously as shown in Fig. 1.9(a). However, in order to implement such super multi-view condition, it is necessary to implement

multiple viewpoints using single panel, so it causes severe resolution reduction [36, 37].

A layered display as shown in Fig. 1.9(b), it physically provides the focus cue with various layered display, and the images on each layered display are processed with various algorithms such as depth-fused display and light field compressive display [38-41].

In particular, a light field compressive display can reduce information loss of the display by compressing the information so that a single pixel shares information of several rays, contrary to the conventional display where a pixel corresponds with only one ray. However, in practice, multi-layered display requires time multiplexing or multiple display, which aggravates the computational load or bulkiness of the system.

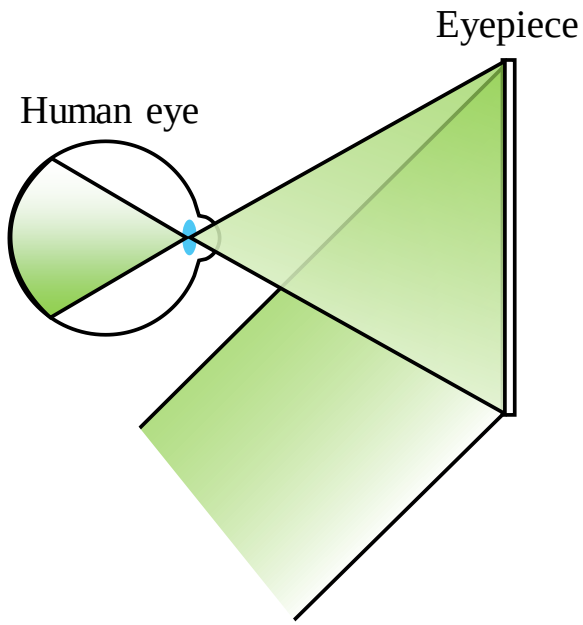

Figure 1.10 Concept of retinal direct projection.

Figure 1.10 shows the retinal direction projection method. In contrast to the general imaging cases like Figs. 1.8 and 1.9, the ray has one to one correspondence with one point in the retina. Thus, it provides a clear image invariant with the human eye lens.

The retinal direct projection system does not provide the focus cue itself, but as an all-in-focus system, has the potential to give a virtual focus cue through proper image processing and eye tracking system. However, the eyebox is extremely limited due to the need to make the ray irrespective of the eye lens, so an additional dynamic eyebox steering technique is required to solve this problem [23].

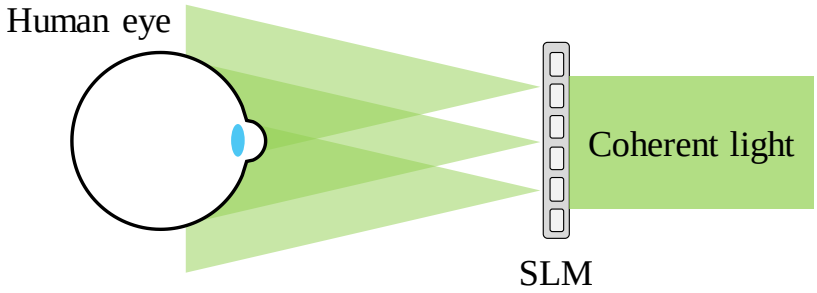

Figure 1.11 Principle of holography.

Holography, which is considered as an ultimate display, reproduces the full wavefront of an object. Figure 1.11 shows the basic principle of holographic display. The holographic display is based on the interference of light, as it reproduces the wavefront of an object using coherent light and a spatial light modulator a shown in Fig. 1.11. The light diffracted by the SLM creates a hologram image, so the typical holographic display can float the image without eyepiece. However, since the diffraction angle of the diffracted light is determined by the pixel pitch of the SLM, with even the most state-of-the-art SLMs comprising a pixel pitch of a few micrometers, the FOV of the typical holographic display is narrow. Therefore, an eyepiece is required to adopt the holographic display in a near-eye display where FOV is very crucial.

1.4 Motivation and contribution of this dissertation

Table 1.1 Comparison of current near-eye display for augmented reality with their characteristics. BS is beam splitter, CM is curved mirror, DHOE is diffuser holographic optical element, and LHOE is lens holographic optical element.

Name	Combiner	Eyepiece	FOV	Eyebox	Transparency	Efficiency
Google glass	BS	CM	Small	Moderate	Moderate	Moderate
Meta 2	Curved mirror		Large	Large	Moderate	Large
Hololens	Waveguide	DOE	Small	Large	High	Small
Free-form	Free-form prism		Small	Moderate	Moderate	Moderate
Retinal 3D (Jang)	Projection	LHOE	Moderate	Small	High	Moderate
Holographic (Maimone)	Projection	LHOE	Large	Small	High	Moderate
IMACL (Ch. 3)	DHOE	IMACL	Moderate	Large	High	Moderate
Metalens (Ch. 4)	BS	Metalens	Large	Large	Low	Small

The display technique, optical eyepiece, and combiners have various combinations depending on the purpose of use and the target specifications. However, neither the bird bath type nor the DOE method has become a game changer that dominates the market, and so, various researches are under way to overcome the shortcomings of each system. Among the various current bottlenecks, this dissertation focuses on the implementing a near-eye display with wide FOV. Large FOV is an essential parameter in providing a more immersive AR with near-eye display. The FOV should be at least 80° to vanish the stereo window but even the most cutting-edge near-eye displays rarely satisfy this criterion. Thus, increasing the FOV without sacrificing

other optical parameters such as the eyebox, the form factor, and eye relief is important in realizing a more realistic AR.

Table 1.1 summarizes the existing commercial near-eye display products and academic studies. Besides the conventional near-eye display for educational and martial purposes, Google glass had been released for commercial purpose on early stage [27]. Due to various efforts on commercialization from the Google glass, various near-eye display for AR have been represented and various studies are continuing from bird bath type products to combination between waveguide and DOE products as discussed in Ch. 1 [22, 24-26]. As shown in Table 1.1, these products are in a trade-off relationship with various elements such as FOV, eyebox, transparency, and efficiency as well as form factor and resolution. Various studies have been conducted to overcome the disadvantages of the systems while maintaining their merits. In academia, an integral imaging and free-form optics has been adopted to provide a high-resolution with low aberration three-dimensional image and mitigate the bulkiness problem of the beam splitter and concave mirror with a free-form optic [29-30]. There have also been lightweight near-eye displays using HOE which adopt light field display and holographic display [23, 33]. Most commercial and academia studies make progress in providing a focus cue and implementing lightweight system, respectively, but have difficulty in providing a FOV of more than 80° in the horizontal direction.

In this dissertation, a near-eye display with a wide field of view over 80° is presented. As a way to realize wide FOV, a concept of transmissive eyepiece is devised in Ch. 2. In Ch. 2, the concept and advantages on FOV

due to the transmissive eyepiece is presented. Especially, it is shown that the transmissive eyepiece can increase the FOV without sacrificing the other performance of the existing system.

In the Ch. 3 and Ch. 4, proposed optical elements are introduced for transmissive eyepiece. In this dissertation, a polarization-multiplexed optical element is used for realizing the transmissive eyepiece. Chapter 3 analyzes the index-matched anisotropic crystal lens comprising an anisotropic crystal and presents a near-eye display comprising the index-matched anisotropic crystal lens. The feasibility of the transmissive eyepiece is verified through the implemented index-matched anisotropic crystal lens and various optical combiners is combined with the eyepiece.

Chapter 4 describes the metasurface as the transmissive eyepiece in order to solve the low numerical aperture (NA) of the index-matched anisotropic crystal due to the small index difference of the anisotropic crystal. With stunning optical characteristics of metasurface lens which incorporates large NA (over 0.6) and thinness, the near-eye display of super wide FOV (over 90°) is realized. In addition, aberrations of the metasurface lens is compensated with the holographic display.

With the proposed optical elements such as index-matched anisotropic crystal and see-through metasurface lens, it is shown that FOV over 80° which is considered bottleneck in existing near-eye display can be realized and it does not affect other performance such as form factor and eyebox compared to existing system. Finally, it is discussed the disadvantages which are low efficiency and transparency due to optical properties of anisotropic crystal and metasurface and discussed ways to solve them.

Chapter 2 Transmissive eyepiece for wide field of view near-eye display

2.1 Transmissive eyepiece for near-eye display

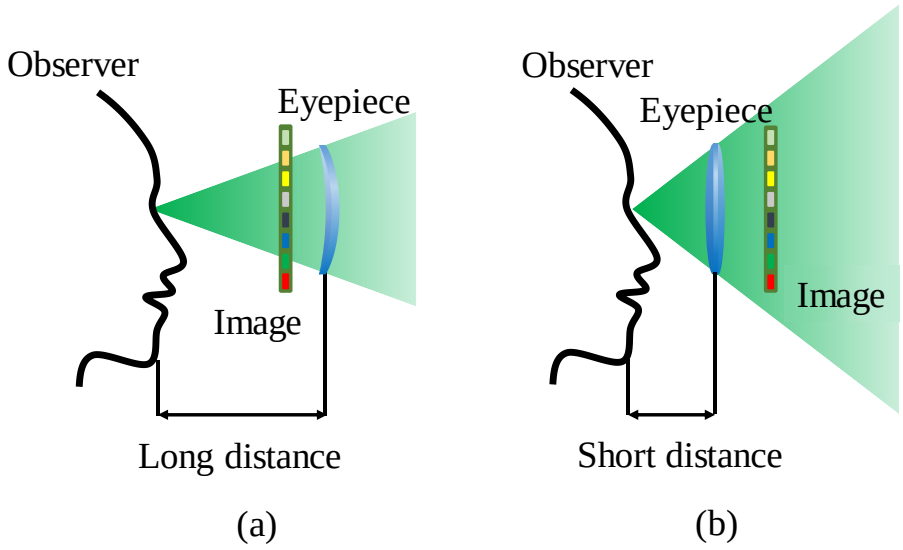

Figure 2.1 Comparison between the reflective eyepiece and the transmissive eyepiece regarding the FOV: (a) reflective eyepiece and (b) transmissive eyepiece.

Figure 2.1 outlines the comparison between the reflective eyepiece and the transmissive eyepiece in terms of the FOV. For the sake of simplicity in the explanation, the optical combiner has been omitted. Since the reflective

eyepiece has long distance between the human eye and the eyepiece, the FOV is narrow as shown in Fig. 2.1(a). On the contrary, the transmissive eyepiece has short distance between the human eye and the eyepiece because the eyepiece is located right in front of human eye, the FOV is relatively wider as shown in Fig. 2.1(b). In other words, near-eye displays using reflective eyepieces, wherein the optical combiners and displays are located between the eyepiece and the human eye, have a smaller FOV due to the structural characteristics.

However, in the reflective eyepiece system, the directions of light from real world and light from virtual information is different, so thin slab concave mirror or reflective optical element can operate differently to the lights. However, the eyepiece is located right in front of the human eye, the lens distorts the light from the real-world scene while floating the virtual information. Therefore, transmissive eyepiece requires multi-functional optical element that operate transparent glasses to the real-world scene and floating lens to the virtual information.

Since the basic principle of the system using the reflective eyepiece and the transmissive eyepiece is identical except for the distance between the human eye and the eyepiece, the display system such as the FOV, the eyebox, and the form factor can be analyzed at the same time as shown in Fig. 2.2.

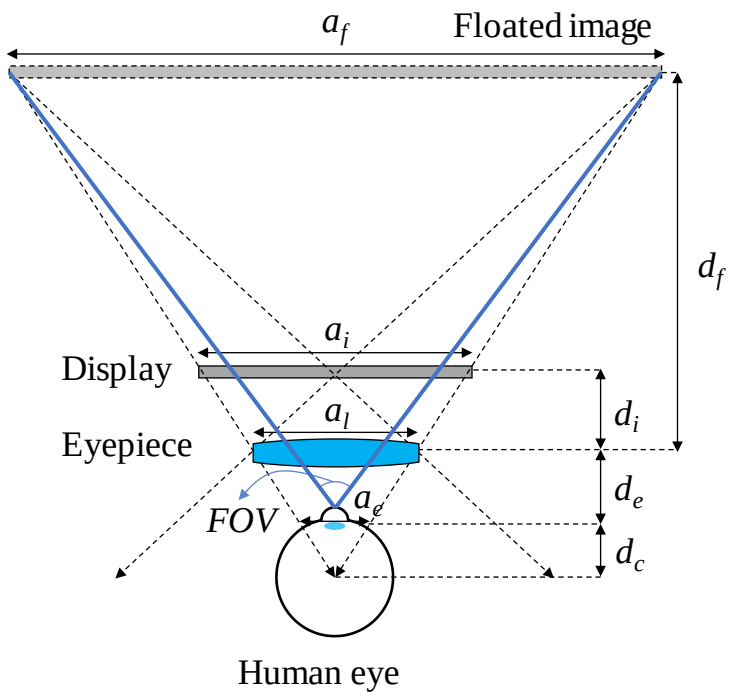

Figure 2.2 Parameters and performances of near-eye display.

The desired floating depth (d_f), lens aperture (a_l), and intended eyebox (a_e) are fixed variables in near-eye display. The FOV, required display size (a_i), and thickness of the system (d_i) is described below:

$$d_c = \frac{a_e d_e}{a_l - a_e}, \tag{2.1}$$

$$a_f = \frac{a_e(d_c + d_e + d_f)}{d_c}, \tag{2.2}$$

where d_c means the converging point, and a_f is the size of floated image,

$$d_i = \frac{f d_f}{d_f + f}, \tag{2.3}$$

$$a_i = \frac{a_f d_i}{d_f}, \tag{2.4}$$

$$FOV = 2\tan\left(\frac{a_f}{d_e + d_f}\right), \tag{2.5}$$

wherein the f is the focal length of the eyepiece.

Figure 2.3 visualizes the various relations between the parameters such as eye relief, eyebox, lens aperture and FOV based on the equations above. The simulation parameter is assumed to have a floating distance of 2000 mm, lens aperture of 35 mm, and eyebox of 5 mm. Eye relief is assumed to 10 mm and distance between the image and eyepiece is added to the eye relief in case of reflective eyepiece.

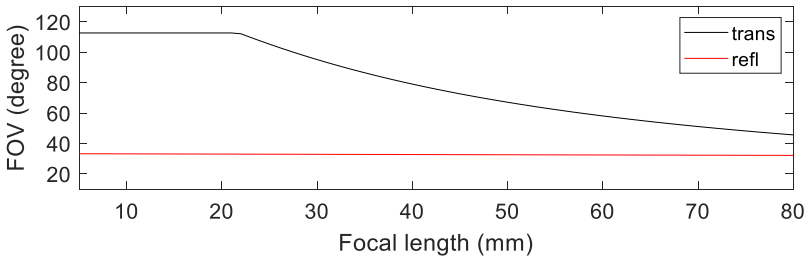

(a)

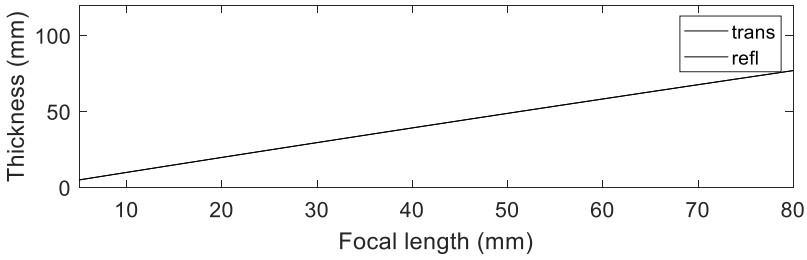

(b)

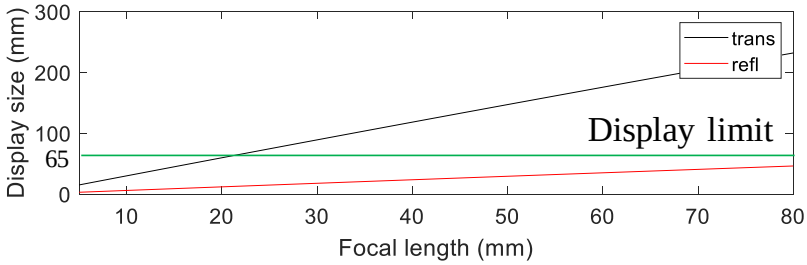

(c)

Figure 2.3 Relation between the near-eye display system parameters: (a) FOV along the focal length of the eyepiece. (b) distance between image and eyepiece which is called thickness of the system, and (c) required display size along the focal length of eyepiece. The display size is limited by interocular distance not to interfere the other display for the other eye. The green line represents the display limit.

The key factors of the performance of the near-eye display under fixed target parameters are the distance between the human eye and eyepiece (d_e), and the focal length of eyepiece. As shown in Fig. 2.3(a), the FOV of transmissive eyepiece is much larger than the one of reflective eyepiece. In certain case, the FOV of transmissive eyepiece is 3 times more than the FOV of the reflective eyepiece. Figure 2.3(b) and (c) shows form factor of the system, thickness and display size. The thickness is defined by the distance between eyepiece and image which is key parameter to determine the thickness of near-eye display. In Fig. 2.3(c), the displays for each eye cannot be larger than the interocular distance of human eye not to interfere each other. Thus, the display limit is set to the 65 mm and it limits the FOV of the system as shown in Fig. 2.3(a). In other words, the FOV of transmissive eyepiece system is limited because it cannot fully utilize its required display size due to the display limit.

Nevertheless, the transmissive eyepiece system provides at most 3 times wider FOV than the reflective eyepiece system by virtue of its structural advantages.

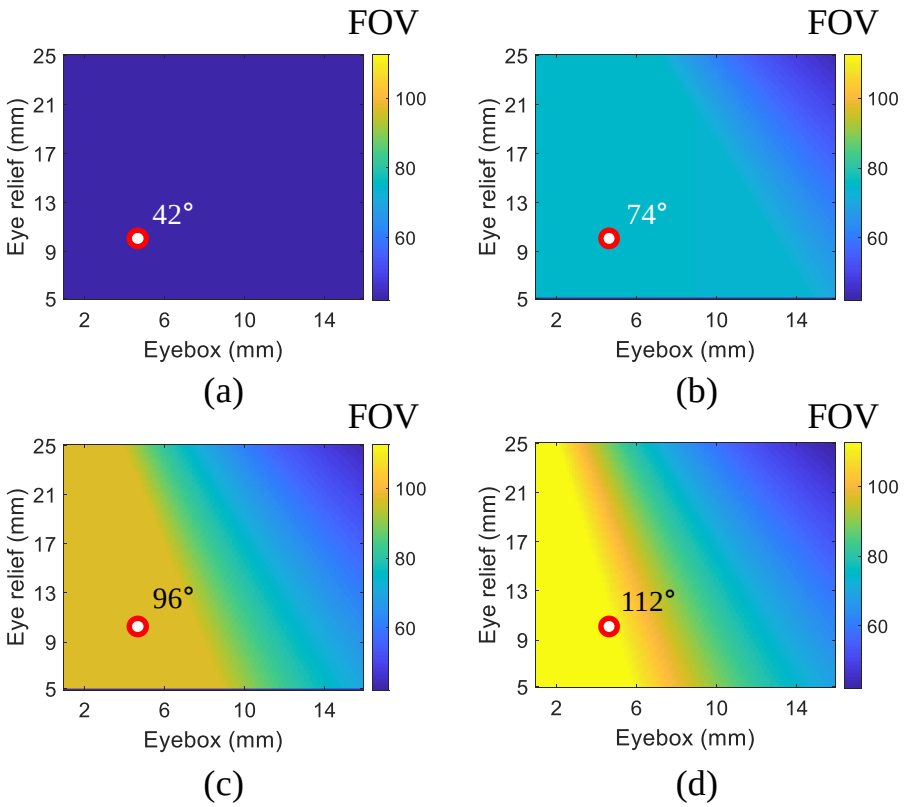

Figure 2.4 Field of view according to various eyebox and eye relief along the different numerical aperture. The lens aperture is assumed to 35 mm. The numerical aperture is (a) 0.2, (b) 0.4, (c) 0.6, and (d) 0.8.

Figure 2.4 shows the FOV according to the various eyebox and eye relief condition in different NA. In the near-eye display, the aperture size of the eyepiece is hard to adjust due to convenient user experience, so the focal length of eyepiece decides the FOV of the system. As shown in the Figs. 2.3 and 2.4, the short focal length, or large NA induces the large FOV under same condition.

Therefore, in order to realize the desired wide FOV in this dissertation, two optical properties are needed. The first is to use a structural advantage of a transmissive eyepiece by devising a multi-functional optical element that responds differently to real world scenes and virtual information located right in front of the eye.

The second is to implement an eyepiece with large NA, or short focal length, to maximize the wide FOV properties of this transmissive eyepiece. In next chapter, it is discussed how to implement these multi-functional optical elements and how to extend the NA of multi-functional optical element.

Chapter 3 Near-eye display using index-matched anisotropic crystal lens

3.1 Introduction

In this chapter, the novel optical combiner, index-matched anisotropic crystal lens (IMACL) is proposed and the near-eye display with IMACL capable of providing large FOV is presented. The lens made of the anisotropic crystal is enveloped with the isotropic material having same curvature of the anisotropic crystal lens. When the refractive index of the isotropic material is same for a certain polarization state of the anisotropic crystal lens, the IMACL functions as a transparent glass or a lens according to the polarization state of the incident light. Using this multi-functional property of the IMACL, the practical near-eye display using the IMACL is demonstrated. The virtual image is polarized to the polarization state of lens mode in IMACL and the real-world image is polarized to the polarization state of the glass mode in IMACL.

There have been various researches utilizing the anisotropic crystal to improve the ability of the three-dimensional (3D) display or HMD [42-44]. In addition, there have also been studies to utilize the polarization selectivity by matching the refractive index of certain polarization axis [45]. However, it is the first time to utilize the index-matched anisotropic crystal lens to realize the see-through near-eye display. The near-eye display using IMACL has the significance not only because it is an initiative study with the novel

structure but also because the FOV and the form factor can be enhanced by the proposed system compared with the conventional near-eye display. Especially, the system using the IMACL has the structure similar to the near-eye display for virtual reality, so the proposed system has the possibility of large FOV. Furthermore, the system using IMACL can be a promising candidate with the development of transparent flat panel like transparent OLED because of the similarity of the structure with the near-eye display for virtual reality.

The proposed eyepiece can be applied not only to simple bird bath systems but also to lightguide system to reduce system bulkiness. A direct projection can also be implemented with a transparent screen to drastically reduce the system bulkiness and weight. The specific contributions covered in this chapter are:

- Design method of index-matched anisotropic crystal lens
- Analysis of aberrations of IMACL
- Analysis of display performance of near-eye display with IMACL
- Implementing the near-eye display with various optical combiner including beam splitter, light guide, and direct projection
- Flat panel type near-eye display using IMACL
- Practical designs and implementation of transparent screen with diffuser holographic optical element

3.2 Index-matched anisotropic crystal lens

3.2.1 Principle of the index-matched anisotropic crystal lens

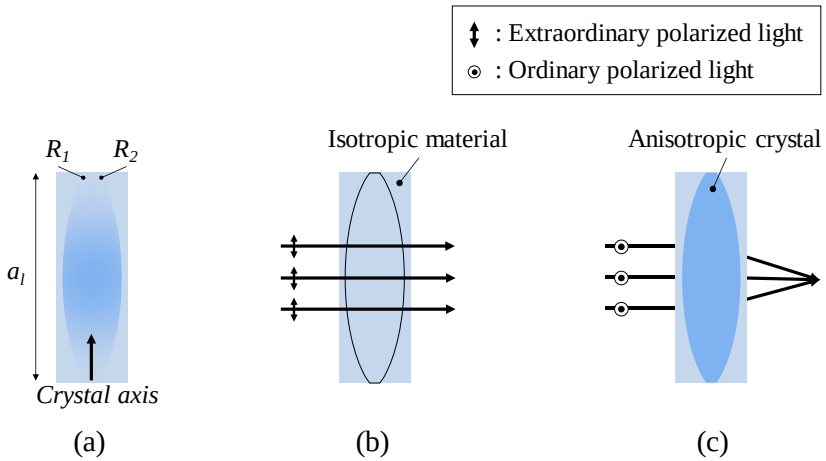

Figure 3.1 Basic concept of index-matched anisotropic crystal lens.

The IMACL is proposed as the multi-function optical element working as glass and lens at the same time. The basic concept of the IMACL is presented in Fig. 3.1. The anisotropic crystal lens is enveloped with the isotropic material which has the same curvature of the anisotropic crystal lens. The refractive index of the isotropic material is matched with the smaller value of the refractive indices of the anisotropic crystal. In case of the positive anisotropic crystal, the isotropic material should have the same refractive index with the ordinary refractive index of the anisotropic crystal, and in case of the negative anisotropic crystal, the isotropic material should have the same refractive index with the extraordinary refractive index of the anisotropic crystal. Figure 3.1(a) represents the basic structure of the IMACL.

The negative anisotropic crystal is assumed and the R_1 and R_2 are the curvature radii of the anisotropic crystal lens and a_l is the aperture size of the anisotropic crystal lens. To show the functionality of the IMACL, the incident light is assumed as parallel rays. The extraordinary-polarized incident rays go through the IMACL without refraction as shown in Fig. 3.1(b) because the refractive indices of isotropic and anisotropic material are same in the extraordinary-polarized light. Meanwhile, the IMACL operates as a lens to the ordinary-polarized incident rays, so the incident rays are focused at the focal plane of the IMACL as shown in Fig. 3.1(c). When the positive anisotropic crystal is used as lens, the basic functionality is same with the Fig. 3.1, but the polarization state of the incident light is reversed compared with the case of the Fig. 3.1. In fabrication step of the anisotropic crystal lens, orientation of crystal axis decides the refractive index of each polarization state of anisotropic crystal. The optical axis of the anisotropic crystal should be perpendicular to the primary direction of the incident light so that the birefringent property of the IMACL is maximized.

The focal length of IMACL is decided by lens curvature and the index difference as follows:

$$\frac{1}{f} = n_i \left(\frac{n_a}{n_i} - 1 \right) \left(\frac{1}{R_1} - \frac{1}{R_2} + \frac{(n_a - n_i)d}{n_a R_1 R_2} \right), \tag{3.1}$$

where n_a and n_i are refractive indices of the anisotropic crystal in lens mode and refractive index of the isotropic medium, respectively, and d is the thickness of the lens. As presented in Eq. (3.1), focal length of the IMACL is

decided by the index difference between the two polarization states of the anisotropic crystal. Therefore, anisotropic crystal having large index difference is recommended to make short focal length of IMACL, because the short focal length of lens guarantees the small form factor.

3.2.2 Aberration analysis of index-matched anisotropic crystal lens

Since the near-eye display using IMACL merges the virtual information with real-world scene in line, there is little aberration compared with the off-axis configuration. However, since the IMACL is made of the anisotropic crystal, aberration is caused by the anisotropy. Especially, in case of the birefringent crystal, refractive index is different according to the angle between the crystal axis and the coordinate, so the astigmatism is the dominant aberration factor [46]. The refractive index of anisotropic material is generally indicated by index ellipsoid, it is well known that the extraordinary refractive index varies depending on the direction of light, while the ordinary refractive index has the same refractive index regardless of the direction of the light. Thus, when the crystal axis of the anisotropic crystal lens is set to the *y*-direction, the focal length in the *x*-direction and the focal length in the *y*-direction become different. There have been studies that show the index deviation induces the astigmatism of the anisotropic crystal lens [47]. The astigmatism due to index deviation in extraordinary refractive index is represented in different types in IMACL according to the kind of anisotropic crystal. The IMACL with positive anisotropic crystal uses

extraordinary-polarized state as lens, so the distortion is represented in lens imaging relation. On the other hands, the IMACL with negative anisotropic crystal uses extraordinary-polarized state as transparent glass, so the distortion is represented in see-through mode. To analyze the aberrations in IMACL, the IMACL is simulated with the Code V [48].

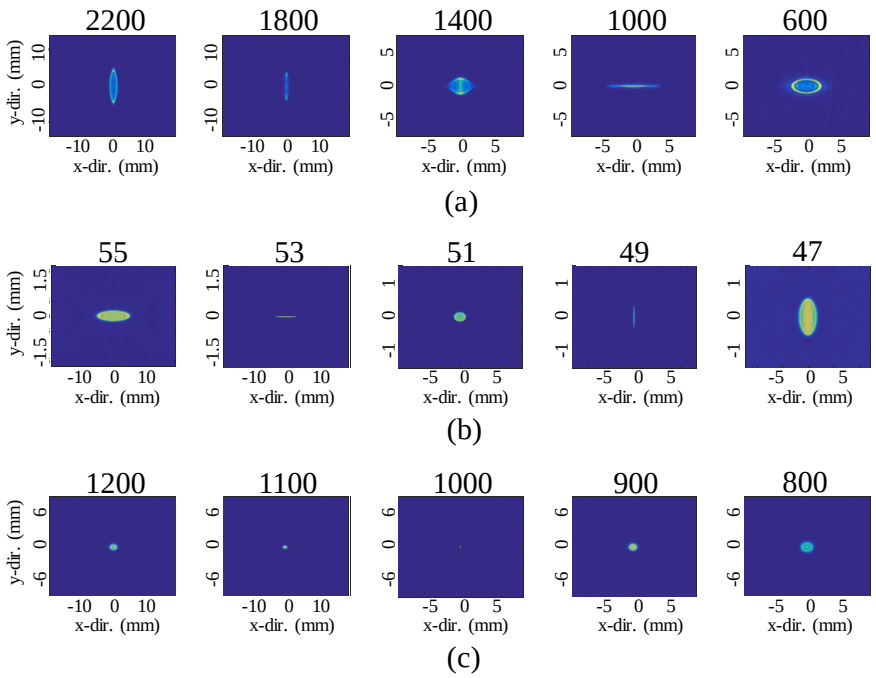

Figure 3.2 Analysis of astigmatism in IMACL: (a) PSF of the IMACL with positive anisotropic crystal in lens mode, (b) PSF of the IMACL with negative anisotropic crystal in see-through mode, and (c) PSF of the IMACL with negative anisotropic crystal in lens mode.

Figure 3.2 shows the point spread function (PSF) of the IMACL. Figure 3.2 (a) shows the PSF of the IMACL with positive anisotropic crystal and Figs. 3.2(b) and (c) show the PSF of the IMACL with negative anisotropic crystal. The refractive indices of each polarization state are 1.2 and 1.6, respectively, and the radius of curvature is 45 mm. Hence, the effective focal length of the lens is formed near the 58 mm. In Fig. 3.2(a), a point light source is located 55 mm behind the IMACL and the PSF is measured in lens mode because the IMACL with positive anisotropic crystal uses the extraordinary-polarized state as lens mode. Figure 3.2(a) shows the PSF variation along the *z*-direction and it is shown that the focal plane of the *x*-direction is formed at the depth of 1000 mm and focal plane of *y*-direction is formed at the depth of 1800 mm. Since the anisotropic crystal in IMACL is birefringent material, the index deviation by the anisotropic property is only represented in *y*-coordinate and it induces the astigmatism of the lens. The distance between focal plane of *x*-direction and *y*-direction is 800 mm which is considerable value in imaging system.

Figures 3.2(b) and (c) show the simulation results of IMACL with negative anisotropic crystal lens. In this case, the IMACL operates as glass in extraordinary-polarized state, so the see-through mode is simulated. In Fig. 3.2(b), the point light source is located 50 mm behind the IMACL and in Fig. 3.2(c), the point light source is located 1000 mm behind the IMACL. The distance between the plane that focuses in the *x*-direction and the plane that focuses in the *y*-direction is only 4 mm when the point light source is located 50 mm behind the IMACL. On the other hand, when the point light source is located far from the IMACL about 1000 mm, the astigmatism and the depth

distortion are negligible. In the simulation specification, the variation of the incident angle to the IMACL is about 20° where the point light source is located 55 mm from the IMACL and it causes the index deviation of 0.068. However, in case that the point light source is located far from the IMACL, the variation of the incident angle is small, and the index deviation rarely affects the image formation. In the simulation specification where the point light source is located 1000 mm behind the IMACL, the index deviation is only 0.00002.

Therefore, IMACL has the small distortion when the image in the long distances is observed through the IMACL with the negative anisotropic crystal. Because the real-world of interest is located at more than 500 mm, astigmatism caused by index deviation can be ignored. Hence, based on the analysis, it can be deduced that the negative anisotropic crystal is more suitable for implementing IMACL.

3.2.3 Implementation

The IMACL is fabricated with calcite ($CaCO_3$) in the experiment which is the representative negative anisotropic crystal. There are various birefringent materials of high index difference including liquid crystal and titanium dioxide (TiO_2) from 0.3 to 0.4, but in this chapter, the calcite is used for verification of the proposed concept due to ease of fabrication. The calcite is immersed in the index matching liquid to implement the IMACL and the refractive index of index matching liquid is 1.486 which is equal to the extraordinary refractive index of the calcite.

Table 3.1 Specification of implemented IMACL.

Lens specification	Value
Diameter (a_l)	20 mm
Radius of curvature (R_1, R_2)	14.98mm
Thickness of the lens (d)	10.64 mm
Extraordinary refractive index of lens (n_e)	1.486
Ordinary refractive index of lens (n_o)	1.658
Refractive index of isotropic material	1.486

As following the Eq. (3.1), the focal length of the IMACL is calculated to be 42 mm and the measured focal length of IMACL is 45 mm. The detailed specification of fabricated IMACL is presented in Table 3.1. In order to verify the fabricated IMACL, the focal length is measured through collimated laser light as shown in Fig. 3.3.

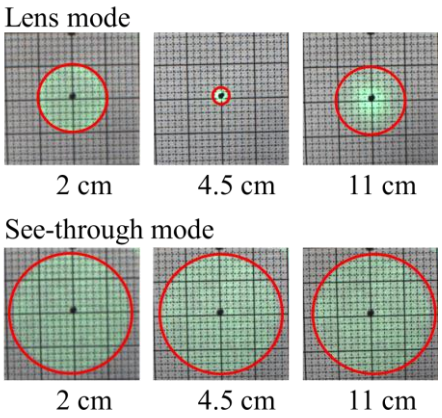

Figure 3.3 Feasibility verification of IMACL.

3.3 Near-eye displays using index-matched anisotropic crystal lens

IMACL can be utilized in various systems due to its novel property that two optical functions can be performed at the same time by the polarization multiplexing. Especially, IMACL can improve various optical performance of the near-eye display with its own characteristic. Especially, it can be applied not only to beam splitter or light guide system but also to direct projection and transparent screen.

3.3.1 Near-eye display using index-matched anisotropic crystal lens

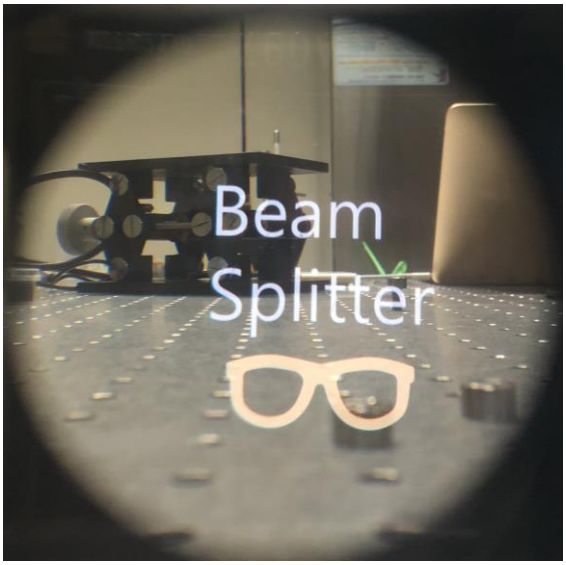

Figure 3.4 Near eye display with beam splitter and IMACL.

Figure 3.4 shows a basic near-eye display implemented using IMACL and beam splitter to verify the feasibility of proposed eyepiece. However, the beam splitter has the disadvantage that the system becomes too bulky because it requires bulky space to enlarge the image. Therefore, to reduce this bulkiness, a lightguide can be adopted instead of beam splitter.

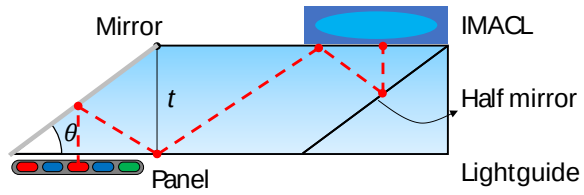

(a)

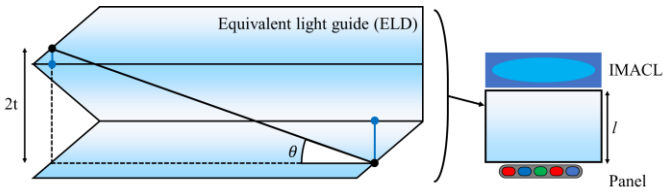

(b)

Figure 3.5 Near-eye display using IMACL with lightguide: (a) illustration of system and (b) design condition of the lightguide.

Figure 3.5 shows near-eye display using IMACL and lightguide. θ means apex angle, and t indicates thickness of lightguide. Lightguide can be simply designed as shown in Fig. 3.5(b). The light from the panel goes through the lightguide and the light guide can be expressed as the transparent slab whose thickness is l. With the equivalent lightguide model, the thickness

l is presented in Eq. (3.2):

$$l = t\left(\frac{2}{\sin(\theta)} + 1\right). \tag{3.2}$$

In general, the length of slab (l) shortens the imaging distance by a refractive index (n) in the paraxial approximation. If the lightguide is designed so that the imaging distance (l/n) is equal to f, the distance between the eyepiece and the display decreases from f to t as presented in Eq. (3.3). For example, assuming an apex angle of 30°, the thickness is reduced by about 3.3 times.

$$t = f\left(\frac{n\sin(\theta)}{2 + \sin(\theta)}\right). \tag{3.3}$$

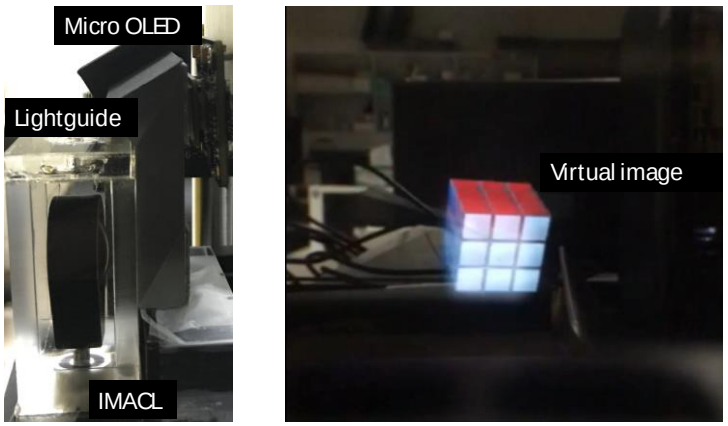

Figure 3.6 Near-eye display prototype with lightguide and IMACL.

Figure 3.6 shows the near-eye display system using the light guide and the results. A prototype is implanted to confirm the feasibility by using the

micro OLED display and the implemented IMACL. The thickness of the light guide is 10 mm and the apex angle is 30°. The size of the micro OLED display in this experiment is small by 25.4 mm (diagonal), so the FOV of 31° is realized when the eye relief is 15 mm and fixed eyebox.

Despite the compact light guide, even the lightguide system is difficult to satisfy socially acceptable criteria due to heavy optical property and bulkiness of lightguide itself. Therefore, the most suitable optical combiner for IMACL to realize the wide FOV is direct projection method using a transparent screen.

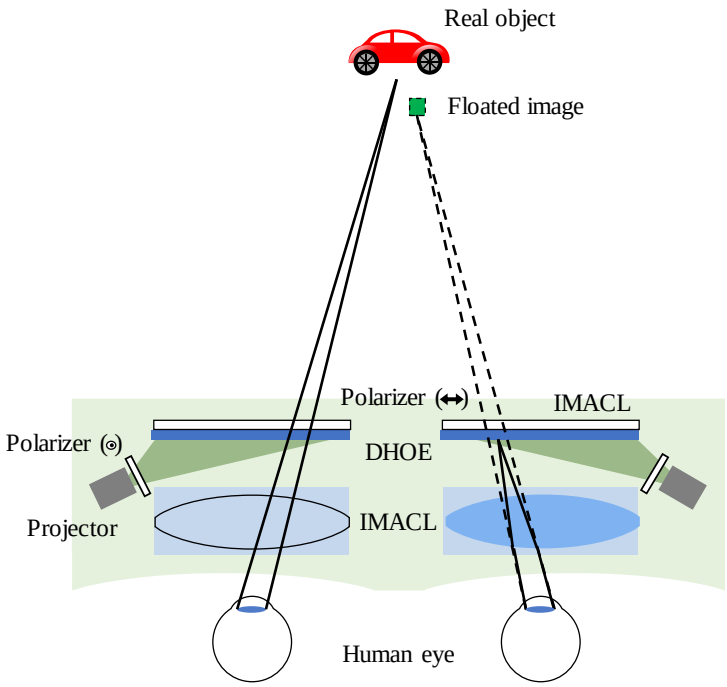

Figure 3.7 Schematic diagram of near-eye display using IMACL and direct projection.

Figure 3.7 shows the basic configuration of the near-eye display using IMACL and direct projection. As shown in Fig. 3.7, rays from the real object are polarized by the extraordinary polarizer located behind the transparent diffuser. The extraordinary-polarized rays from the real object are not refracted by the IMACL, so the see-through real-world information can be observed. Meanwhile, the rays from projector are ordinary-polarized by the polarizer and diffused by the transparent diffuser. The diffused ordinary-polarized light is focused by the IMACL and user can observe the floated image. As a transparent diffuser, diffuser holographic optical element (DHOE), index-matched diffuser, and scattering polarizer can be good candidates [49-52]. Among them, since the DHOE shows real-world scene with high transmittance due to its angular selectivity, a DHOE is adopted as a transparent diffuser in this scheme. The optical property and the principle of the DHOE is covered in chapter 3.3.3.

As shown in the Fig. 2.3, the FOV and the form factor of the near-eye display using IMACL are decided by various factors such as focal length of the IMACL (f), aperture size of the IMACL (a_l), eye relief (d_e), eyebox (a_e) and desired floating distance (d_f). In general, the form factor of the near-eye display is related to the projection module and the thickness of the optical module. In this chapter, the thickness of the eyepiece does not refer to the thickness of the IMACL itself, but to the distance between IMACL and the DHOE which is the minimum distance for the IMACL to float image to desired depth.

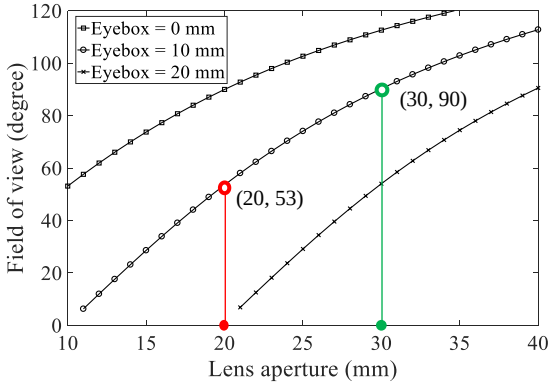
Eyebox = 0 mm
Eyebox = 10 mm
Eyebox = 20 mm
(30, 90)
(20, 53)
Field of view (degree)
Lens aperture (mm)
0
20
40
60
80
100
120
10
15
20
25
30
35
40

(a)

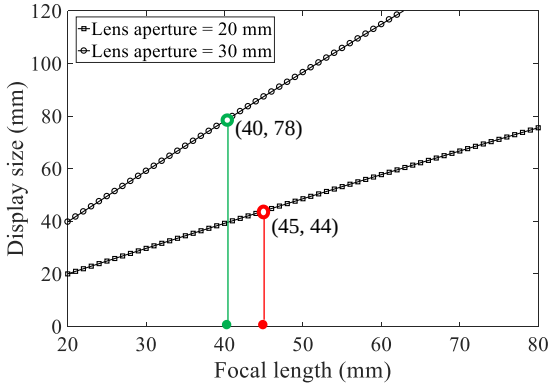
Lens aperture = 20 mm
Lens aperture = 30 mm
(40, 78)
(45, 44)
Display size (mm)
Focal length (mm)
0
20
40
60
80
100
120
20
30
40
50
60
70
80

(b)

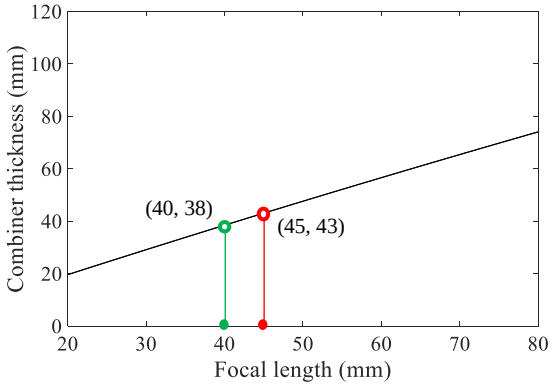
(40, 38)
(45, 43)
Combiner thickness (mm)
Focal length (mm)
0
20
40
60
80
100
120
20
30
40
50
60
70
80

(c)

Figure 3.8 System performance of near-eye display using IMACL with direct projection: (a) FOV according to the lens aperture, (b) required display size according to the focal length of eyepiece and (c) thickness of near-eye display along the focal length of eyepiece. The red and green points represent ideal case and implemented IMACL in this dissertation.

Figure 3.8 visualizes the key factors of the proposed near-eye display such as FOV, thickness of combiner and required display size based on above equations. The eye relief of 10 mm and the floating depth of 1000 mm are assumed. Figure 3.8(a) shows the relationship between lens aperture and FOV for various eyebox based on Eq. (2.5). As shown in Eq. (2.5), the FOV of the proposed system is determined by the lens aperture and the eyebox. The FOV is in trade-off relation with the eyebox, and the large lens aperture guarantees wide FOV. The eyebox is area where the image from display can be seen without loss when the human eye is placed on the eye relief as shown in Fig. 3.8(a). Therefore, when the eyebox of the system is set wide, the FOV decreases because the active area of the display which can provide the image to the human eye becomes narrow. Figures 3.8(b) and (c) show the size of the display required to obtain the full FOV and the distance between the IMACL and the DHOE required to float the image at the desired depth according to the focal length of the IMACL. The display size presented in Fig. 3.8(b) is required to obtain the maximum FOV. If the display size becomes smaller than this value, FOV of the system becomes lower. Figure 3.8(c) shows the thickness of the combiner according to the focal length. In general, for a near-eye display that reproduces images at 1 m or more, the

combiner thickness has a value near the focal length.

Therefore, at a given eye relief and desired floating depth, the FOV of the proposed system is in a trade-off relationship with the eyebox and increases as the size of the lens aperture increases. Meanwhile, under certain lens apertures, the focal length of IMACL is determined by the index difference. The focal length determines the display size and the thickness of optical combiner that are related to the form factor of the system. Thus, short focal length is required to achieve small display size and optical combiner thickness. Therefore, the performance of the proposed system is maximized when IMACL has large lens aperture and short focal length, which are obtained from anisotropic crystal with high index difference. Thus, the proposed system requires the anisotropic crystal with high index difference.

The red point and the green point are examples of the proposed system. The red point is an example used as a test bed in this paper and the green point is an example of ideal case. For the red point, we assumed an IMACL with a lens aperture of 20 mm and a focal length of 45 mm at index difference of 0.17. This allows the system to have FOV of 90° when the eyebox is 0 mm and FOV of 53° when the eyebox is 10 mm. The display size required to implement the system with eyebox of 10 mm and FOV of 53° is 44 mm and the thickness of the optical combiner is 43 mm. For the green point, we assumed an IMACL with a lens aperture of 30 mm and a focal length of 40 mm at index difference of 0.3. This allows the system with FOV of 112° when the eyebox is 0 mm and FOV of 90° when the eyebox is 10 mm. The display size required to implement the system with eyebox of 10 mm and FOV of 78° is 38 mm and the thickness of the optical combiner is

43 mm.

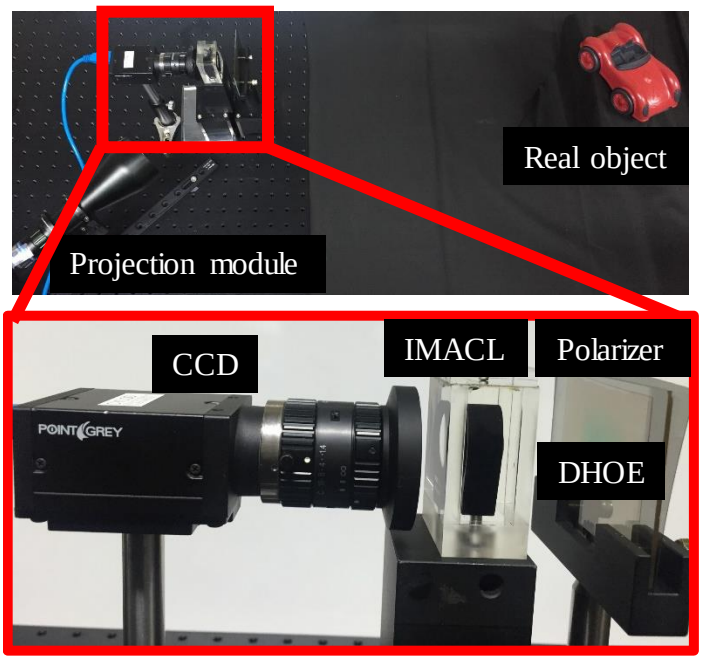

Figure 3.9 Experimental setup of near-eye display using IMACL with direct projection.

Figure 3.9 represents the experimental setup of the proposed see-through near-eye display with direct projection. As a transparent screen, the DHOE is adopted and light from the projector is collimated to coincide the reconstruction condition with the recording condition. The detailed specification of the experimental setup is presented in Table 3.2.

Table 3.2 Specification of near-eye display using IMACL with direct projection.

System specification	Value
Resolution of the projector	1920 (H) × 1080(V)
Thickness of the optical combiner	43 mm
Display (DHOE) size (eyebox of 0 mm)	87 mm (required), 50 mm (experiments)
Display (DHOE) size (eyebox of 10 mm)	44 mm (required), 50 mm (experiments)
FOV (eyebox of 0 mm)	90° (achievable), 53° (experiments)
FOV (eyebox of 10 mm)	53° (achievable), 53° (experiments)
Transmittance	31 %

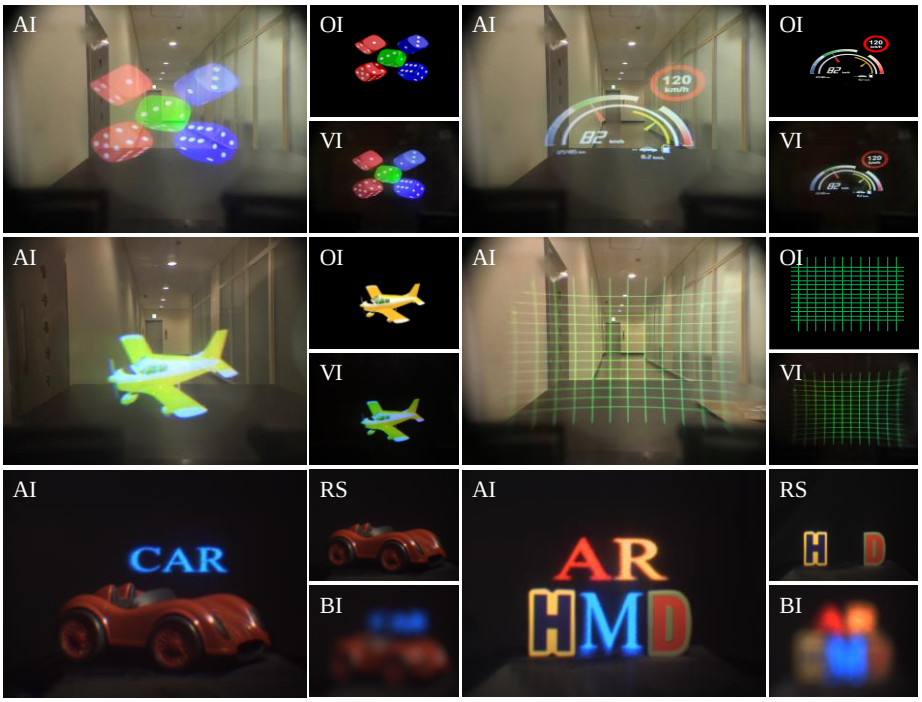

Figure 3.10 Experimental results of the near-eye display using IMACL with direct projection. AI is augmented image, OI is original computer-generated image, VI is virtual image. RS is real-world scene and BI is blurred image.

The distance between IMACL and DHOE is about 43 mm, so the projected image on the DHOE is floated on the 1000 mm away from the IMACL. Figure 3.10 shows the visualization results with near-eye display using IMACL with direct projection. The dashboard, dices, stripes, and plane are augmented to the real object. The images are floated on the plane of the real object which is 1000 mm away from the observer. The four upper images with dices, dashboard, plane and stripes are captured by the camera (iPhone 7, Apple) and the camera is located in eye relief (10 mm). With the DHOE and the IMACL, the full color virtual information is reconstructed. To

show the floated image clearly, the virtual information (VI) is shown by blocking the real-world scene as well as the merged image. Two bottom images with letters are captured by the charge-coupled device (CCD) with lens of narrow depth of field to show the position of the virtual information. The real objects (red car, letters 'H' and 'D') are located in 1000 mm away from IMACL. The virtual information and the real object have almost same blurring effect and they are focused identically.

As shown in Fig. 3.8(c), the display size is important to provide the maximum FOV of the proposed system. The display size depends on the size of the projected image and the size of DHOE. In the laboratory environment, the maximum recording size of the DHOE is about 50 mm, and the maximum size of projected image from the projector is also about 50 mm. Since Fig. 3.10 is captured at a fixed camera position (eyebox of 0 mm), the display size for FOV of 90° should be at least 87 mm. However, as the display size and projected area are limited to 50 mm, the FOV of our prototype is limited to 60°. On the other hand, the maximum FOV is 53° with required DHOE size of 43 mm when the eyebox is 10 mm. In other words, our experimental prototype has the limitation to show the maximum FOV when the camera is fixed (eyebox of 0 mm), but it has enough display size for the eyebox of 10 mm.

As presented above, since the near-eye display system using IMACL is similar with the near-eye display for virtual reality, the IMACL will become worthy of notice with the development of the transparent display. The concept of the flat panel type near-eye display is also proposed, and the feasibility of the system is shown in following chapter.

3.3.2 Flat panel type near-eye display using IMACL

In this chapter, the concept of the flat panel type near-eye display is presented using the IMACL. As improving the transparency of the flat panel, the proposed system using IMACL can be a good candidate for ultimate near-eye display. However, in current stage, the flat panel does not guarantee the enough transparency, so the concept and feasibility of the system is shown. Flat panel type near-eye display can have an advantage of lightweight and compact system because it does not require the projection distance and projection module. However, since it is hard to separate the virtual information on the flat panel and the real-world scene, there are little approaches to realize the flat panel type near-eye display [53].

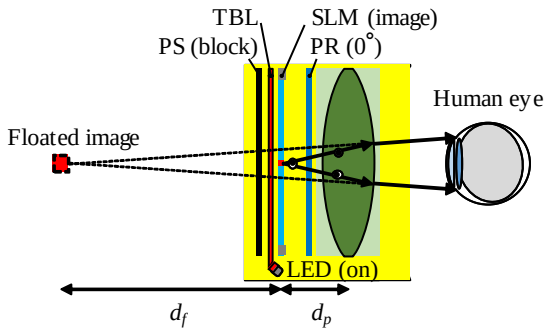

(a)

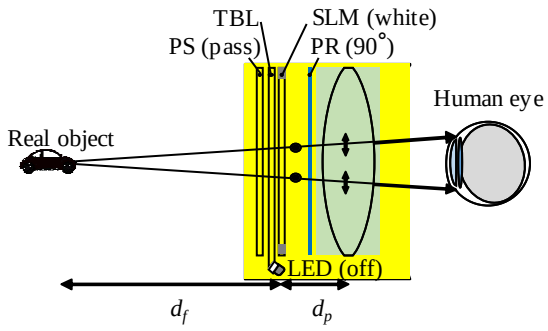

(b)

Figure 3.11 Basic principle of the flat panel type near-eye display with IMACL: (a) shows the principle for virtual information to float and (b) shows the see-through mode.

Figure 3.11(a) and (b) show the schematic diagram of the proposed flat panel type near-eye display. The system is composed of IMACL, polarization rotator (PR), polarization switch (PS), LC panel, and the transparent backlight (TBL). The polarization rotator located in front of the IMACL divides the frame to the see-through frame and the lens frame. At the see-

through frame in the Fig. 3.11(b), the polarization rotator rotates the incident light to the extraordinary-polarized light and at the lens frame, it rotates the incident light to the ordinary-polarized light. Hence, at the see-through frame, the LC panel provides the white image to transmit the light and extraordinary-polarized transmitted light by the polarization rotator goes through the IMACL without any refraction. Meanwhile, at the lens frame, the LC panel provides the virtual information which is floated to the infinity or near the real object by the IMACL because the polarization rotator makes the polarization state of the light from the LC panel to the ordinary polarization state. The polarization switcher located in front of the SLM is extraordinary polarizer to show the real-world scene clearly at the see-through frame and ordinary polarizer to block the outside information at the lens frame. With this time-multiplexing method, the real-world scene and the virtual information is combined. In the lens mode of the IMACL by the polarization rotator, the SLM shows the image set of each color channel. Images for red, green and blue is divided and displayed at each frame. In the glass mode of the IMACL by the polarization rotator, the SLM shows the white image to transmit the incident light from real-world scene. With the time-multiplexing technique, these four frames are merged and makes full color image. In case of monochrome realization, the monochrome image and the white image are alternately displayed. The full color realization sacrifices the image frame of 25% and monochrome realization sacrifices the image frame of 50%.

The TBL is implemented with the transparent diffuser similar with the transparent anisotropic diffuser (TAD) and convex-half-mirror array

(CHMA) [51-52]. As a transparent diffuser, the TBL transmits the real-world scene and reflects the light emitting diodes (LEDs) light.

The image is floated to the infinity at the focal length of the IMACL and so, the focal length decides the form factor. When the focal length of the IMACL is short, the distance between display and the IMACL can decrease and the size of the display to cover full FOV also decreases and it increases the compactness of the system.

The resolution of the system is decided by the resolution of the flat panel. However, in current stage, the flat panel consists of the pixel structure which induces the diffraction effect and it makes the resolution limitation. The LC panel is transparent basically, but the black matrix of the LC panel decreases the transparency and incident light from the real-world scene is diffracted by the pixel structure. The diffraction effect becomes severe as smaller pitch of the pixel structure has and it degrades the see-through property. Therefore, the flat panel type near-eye display has the resolution limitation with the pixel structure LC panel.

The transmittance is also crucial point of the near-eye display. Transmittance is the ratio of how much does incident light from the real-world scene to the observer. The transmittance of the flat panel type system is limited by the transmittance of each device (SLM, polarization rotator, polarization switch, and IMACL). The IMACL operates in certain polarization state, so the incident light should be polarized, and it reduces the transmittance by 50%. In addition, the time-multiplexing technique is used in the system, the transmittance decreases by multiplexing ratio.

The time-multiplexing and the resolution limit of the pixel structure

may hinder the sufficient AR experience in current stage. However, since every optical component including the display module is located in front of the eye in-line, the flat panel type near-eye display using IMACL has compact system configuration. Also, the proposed flat panel type near-eye display system can be utilized more with the development of the transparent flat panel technology like transparent OLED. The experimental setup is shown in Fig. 3.12.

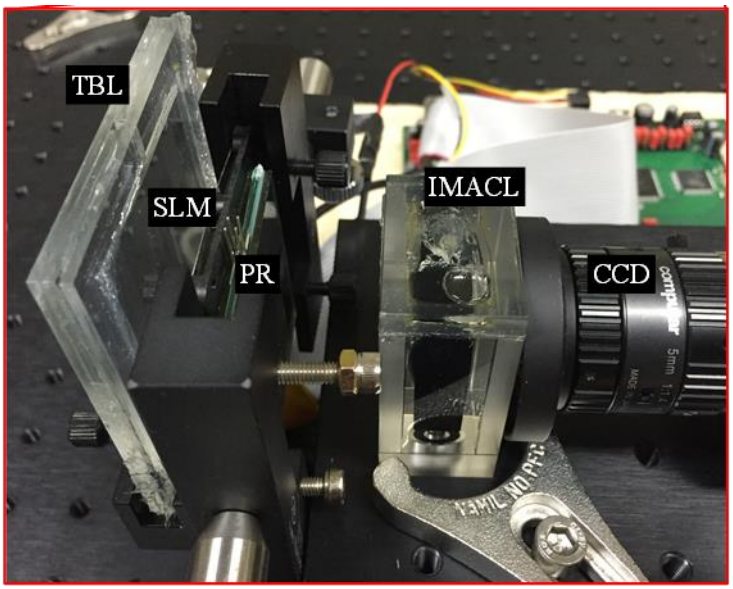

Figure 3.12 Experimental setup of proposed flat panel type near-eye display for augmented reality.

Table 3.3 Specification of flat panel type near-eye display.

System specification	Value
Panel resolution	1024 (H) × 768(V)
Panel pixel pitch	32
Distance between IMACL and panel	40 mm
Distance between real object and IMACL	357 mm
FOV	52 °
Framerate	28 Hz
Transmittance	5 %

The TBL which consists of waveguide and metal coated index matched diffuser is located behind the system. IMACL is located 40 mm in front of the SLM to float the image in the 350 mm away. Figure 3.13 shows the experimental results. The bird and airplane which are virtually overlapped in the real-world scene are floated on the plane where the car and lion are located. The framerate of the display system is measured about 28fps and transmittance of the system is measured to 5%. The polarization rotator (PR), SLM, and LED is synchronized using the PR controller, Arduino, and Video Electronics Standards Association (VESA) signal. The detailed specification of proposed system is shown in Table 3.3. As shown in the Fig. 3.13, the lion and the car are distorted by the diffraction effect.

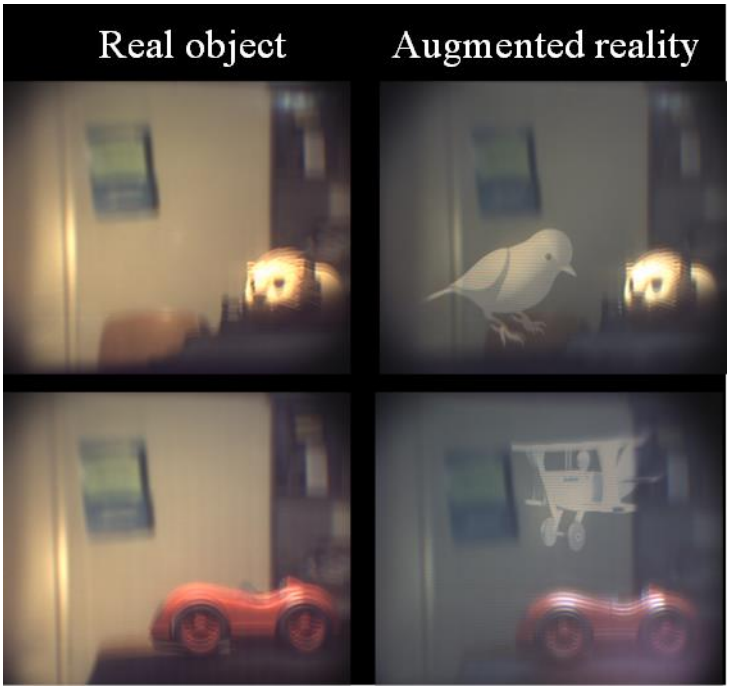

Figure 3.13 Experimental results of proposed flat panel type near-eye display for augmented reality.

3.3.3 Polarization property of transparent screen

As discussed in the previous chapter, HOE records the interference pattern of the light on the photoreactive material. A variety of optical elements have been recorded for HOE including mirror, lens and lens array. In addition, photopolymer, one of the widely used photoreactive material, is often used in see-through applications because of its high transparency [49, 50]. The HOE using photopolymer can also be used to make transparent screens which is called DHOE. The DHOE is used as a promising transparent screen due to its transparency and scattering properties.

In this chapter, the DHOE is adopted as the transparent screen to implement the near-eye display with IMACL. The polarization characteristics of DHOE are important because the IMACL operates selectively to the polarized light. In the previous studies, the polarization properties of holographic diffuser are already analyzed, and it is known that the holographic diffuser can preserve the polarization state [54]. However, in this chapter, the polarization property of the DHOE as the transparent screen is experimentally verified according to the incident angle and diffusing angle.

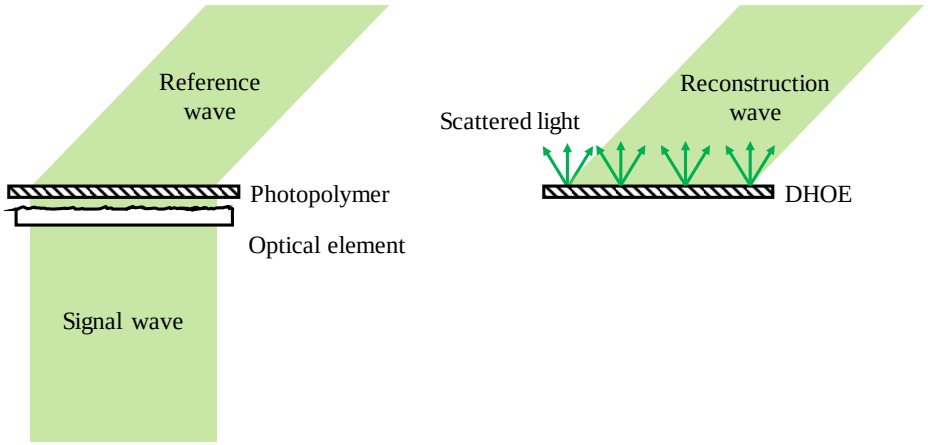

Figure 3.14 Recording and reconstruction process of holographic optical element.

DHOE records and reproduces in the same way as conventional HOE as shown in Fig. 3.14. Figure 3.14 shows a typical HOE recording method. In order to record the interference pattern of the laser light, a signal wave and a reference wave are incident to the photopolymer. The signal wave is modulated to the desired wavefront by positioning an optical element in front

of photopolymer, and a reference wave can be a spherical wave or a plane wave, depending on the display method.

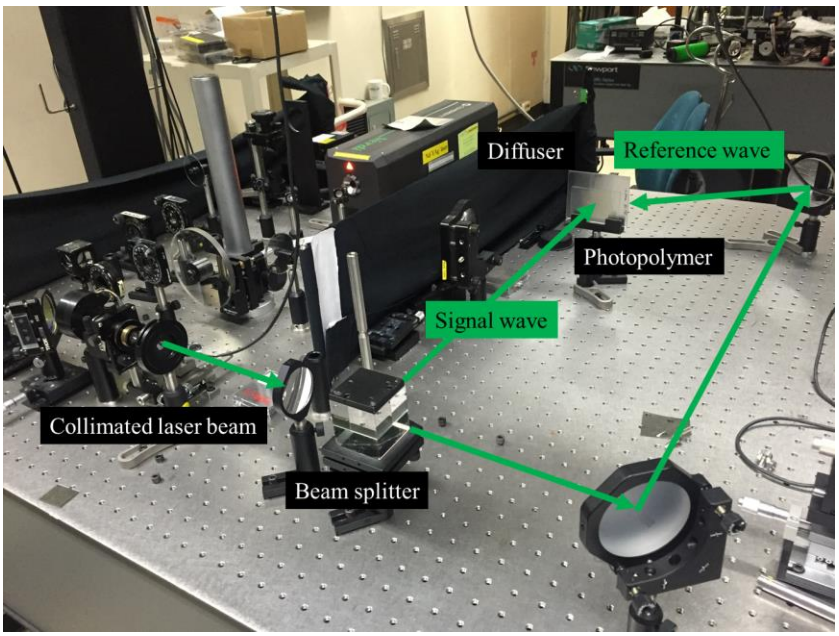

Figure 3.15 Experimental setup of diffuser optical element.

A diffuser is located in front of the photopolymer as shown in Fig. 3.15. Like conventional mirror HOE, the DHOE is based on the volume grating, so it has an angular selectivity and is optically transparent. Therefore, it can be used as the transparent screen in proposed near-eye display with IMACL, under the assumption of that the DHOE preserves the polarization state. Thus, Fig. 3.16 shows the verification of polarization property of DHOE.

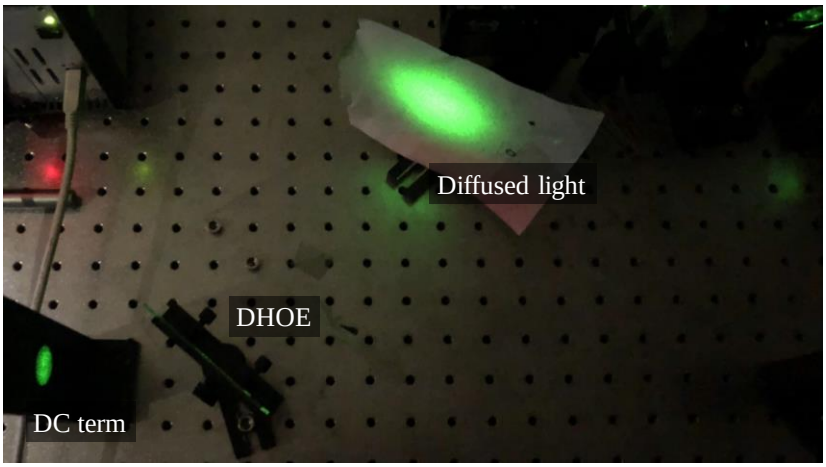

(a)

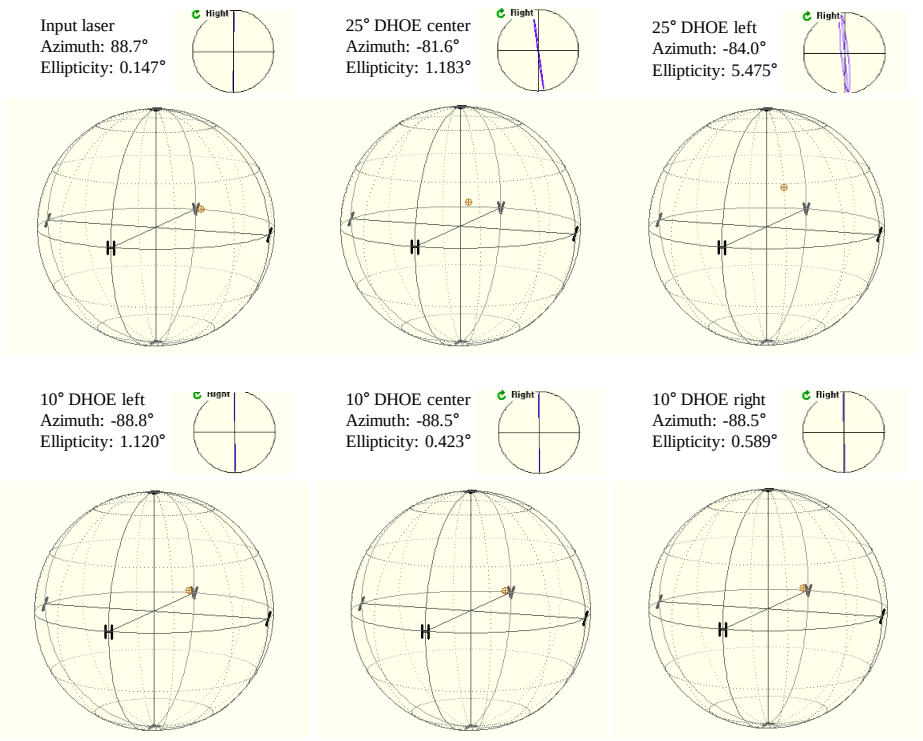

(b)

Figure 3.16 Polarization property of DHOE: (a) experimental setup and (b) polarization properties of various DHOE according to the diffusing angle and

position.

The polarization characteristics of the recorded DHOE as shown in Fig. 3.16(a) are measured using a laser light and a polarimeter. To verify whether the conservation of polarized light differs according to the scattering angle of DHOE, the polarization is measured with DHOE having a scattering angle of 10° and DHOE having a scattering angle of 25°. The diffuser with scattering angle of 10° is well preserved in polarization regardless of the scattering angle. On the other hands, in case of the diffuser having the scattering angle of 25°, but even in the case of 25° DHOE, the scattered light has ellipticity of less than 5°; the polarization state is not severely broken.

3.4 Conclusion

The eyepiece which is called IMACL to realize the near-eye display for AR has been proposed in this chapter. The IMACL is made of the anisotropic crystal lens enveloped with the isotropic material. Hence, the IMACL can be a multi-function optical element according to the polarization state. Because of the property of the IMACL, the IMACL can be located in line with the human eye as an eyepiece. With the proposed near-eye display, the large FOV can be realized. The calcite is used as anisotropic crystal and the FOV of the prototype reaches up to 60°. The FOV can be increased by using the high index difference anisotropic crystal, but the calcite which is relatively high index difference material provides index difference of 0.17. Comparing with the ordinary lens case where index difference between air and glass is 0.5, it is insufficient, and thus, the focal length of proposed IMACL is not

small enough. The FOV is limited by this small index difference, so high index difference anisotropic material should be adopted to the polarization selective optical element.

Chapter 4 Near-eye display using metasurface lens

4.1 Introduction

Metasurfaces are planar optical elements composed of artificially fabricated subwavelength structures, and they have attracted considerable interest owing to their powerful and versatile performance in modifying electromagnetic characteristics [55-59]. Recent advances in metasurfaces show that they can overcome the limitations of conventional bulky optical components, which have restricted the further development of miniature optical and electronic devices [60-66]. Among the various types of metasurfaces, metasurface lenses, also called metasurface lens, are regarded as promising metasurface platforms with great potential for practical application. Thus, pioneering works addressing various concepts related to metasurface lenses have been reported in recent years. For instance, dielectric metasurfaces composed of silicon posts enable the realization of metasurface lenses with high NAs and polarization-selective multi-functional metasurfaces under linearly polarized light [67, 68]. Metasurface lenses based on the spin-rotation coupling of light also exhibit remarkable performance with broadband characteristics [69-72]. Thanks to the high performance and compactness of such metasurface lens, very recent progress in the field of metasurfaces has revealed the potential of metasurface lens for use in future optical devices.

In this chapter, a new metasurface application is proposed for near-eye display for AR that has not yet been reported. Similar with the previous chapter, a display placed in front of a human eye produces a virtual image and allows the user to naturally experience a mixture of virtual information and the real-world. The novel metasurface application that enables a near-eye display with an ultra-wide FOV, full-colour imaging, high resolution and the sufficiently large eyebox is proposed in the chapter. To this end, a see-through metasurface lens with a high NA, a large-area, broadband characteristics, and an engineered anisotropic optical response is proposed. By virtue of the anisotropic optical response, the see-through metasurface lens can perform two different optical functions: it can serve as an imaging lens for virtual information and as transparent glass through which to view a real-world scene. Since these two optical functions can be provided at the same time, the see-through metasurface lens can be positioned right in front of the eye without any optical components like conventional glasses. Thus, it has a much wider FOV than conventional see-through near-eye displays under the same conditions. In other words, the principle of the display is same with the display system proposed in Ch. 2 with IMACL. However, the IMACL has the limitation of small NA due to the limited index difference. On the other hands, the metasurface can provide a compact and wider FOV compared to the display system with IMACL because it can even provide larger NA than the conventional lenses.

To fully utilize this advantage, the metasurface lens has been customized to satisfy the criteria for AR applications. A see-through near-eye display with the see-through metasurface lens with high transmission and

enough modulation efficiency throughout the entire visible region is implemented. Based on this, a wide FOV (90°) is experimentally realized in the prototype display system. In addition, by increasing the lens diameter by 35 mm, the FOV can be increased to more than 120°, which has been regarded as an impossible area in conventional AR display. This work is expected to be a significant advance in many areas including wearable devices, future optical displays, computer vision, wearable electronics, biological imaging, medical devices, and optical microscopy. Moreover, it is worth noting that this research demonstrates the great potential of metasurfaces for practical application in daily lives.

4.2 See-through metasurface lens

4.2.1 Metasurface lens

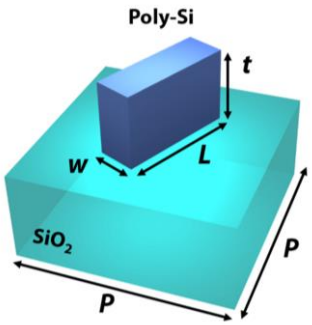

Figure 4.1 Unit cell of nanorod structure metasurface.

As discussed in the previous chapter, a transmission-type eyepiece with a high NA and a large area is required to successfully achieve a wide FOV. In this chapter, a dielectric metasurface with arbitrarily engineered anisotropy

throughout the entire visible region is elaborately designed at the subwavelength scale to satisfy the conditions described above for the transmission-type eyepiece. A schematic illustration of the unit cell of the proposed metasurface is presented in Fig. 4.1. Theoretically, the rectangular dielectric nanorod with an arbitrary orientation angle can be modelled as a Jones Matrix T. An arbitrarily anisotropic nanorod can be represented by a Jones matrix within the coordinates consisting of a longer optical axis and a shorter optical axis, and the Jones matrix can be described as follow:

$$J = \begin{pmatrix} t_l & 0 \\ 0 & t_s \end{pmatrix}, \tag{4.1}$$

where the t_l and t_s are the complex coefficients for longer and shorter optical axis, respectively. Therefore, using the coordinate rotation, the Jones matrix of anisotropic nanorods having arbitrary orientation is

$$T = R(-\theta) J R(\theta) = \begin{pmatrix} \cos\theta & \sin\theta \\ -\sin\theta & \cos\theta \end{pmatrix} \begin{pmatrix} t_l & 0 \\ 0 & t_s \end{pmatrix} \begin{pmatrix} \cos\theta & -\sin\theta \\ \sin\theta & \cos\theta \end{pmatrix}, \tag{4.2}$$

where θ is the orientation angle of the nanorod, and R(θ) is the rotation matrix. In case of the circularly polarized incidence with σ (where σ=1 or -1 for right or left circular polarization, respectively), the complex transmittance from the nanorod can be calculated using the Jones matrix T as follows:

$$E_t = T|\sigma\rangle = \begin{pmatrix} t_l\cos^2\theta + t_s\sin^2\theta + j\sigma(t_s - t_l)\sin\theta\cos\theta \\ (t_s - t_l)\sin\theta\cos\theta + j\sigma(t_l\sin^2\theta + t_s\cos^2\theta) \end{pmatrix}$$

$$= \frac{t_l + t_s}{2}|\sigma\rangle + \frac{t_l - t_s}{2}e^{\mp j2\sigma\theta}|-\sigma\rangle, \qquad (4.3)$$

where the Jones vectors for circular polarization is represented $|\pm\sigma\rangle = [1 \pm j\sigma]^T / \sqrt{2}$. As shown in the right side of Eq. (4.3), complex transmittance for circularly polarized incidence is composed of two orthogonal components with their own complex amplitudes while the phase delay through the orientation angle only exists in cross-polarized components.

To design a metasurface that acts as a spherical lens with a focal length of f for the cross-polarized transmission mode, each unit cell of the metasurface is designed by encoding a spatial phase distribution with the following relation:

$$\theta(x, y) = \frac{\pi}{\lambda}(f - \sqrt{x^2 + y^2 + f^2}), \qquad (4.4)$$

where x and y are the positions in metasurface lens, respectively, and $\theta(x, y)$ is the orientation angle of the nanorod at the position (x, y). Since the co-polarized light is irrelevant to the rod structure as presented in Eq. (4.3), the proposed metasurface lens works as the transparent glass for co-polarized

light, but cross-polarized light undergoes the phase distribution presented in Eq. (4.4). Using the properties of this metasurface, an additional polarizer like Fig. 4.2 is needed to operate as different optical elements according to polarization like IMACL.

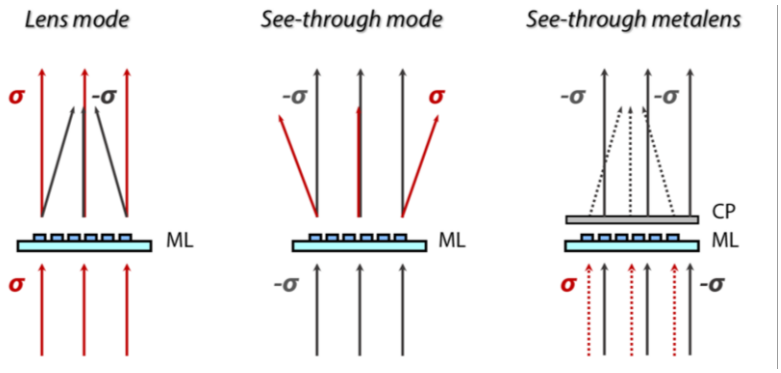

Figure 4.2 Principles of a see-through metasurface lens: (a) incident light with a handedness of σ, (b) incident light with a handedness of (-σ), and (c) the principle of a see-through metasurface lens. ML is metalens, and CP is circular polarization.

Figure 4.2 shows a situation where two circularly polarized lights with different handednesses are incident to the metasurface with the phase distribution as in Eq. (4.4). As shown in Figs. 4.2(a) and (b), in case of incident light with a handedness of σ, metasurface works as transparent glass for co-polarization and convex lens for cross-polarization. Meanwhile, for the incident light with a handedness of (-σ), the metasurface works as a concave lens for co-polarization, but works as transparent glass for cross-

polarization. Using the characteristics of the metasurface that responds differently to these two circularly polarized lights with different handedness, the (-σ) polarizer is used as shown in Fig. 4.2(c). If the cross-polarized component with handedness of (-σ) and co-polarized component with handedness of σ are blocked, it becomes polarization selective eyepiece that reacts with a lens for certain polarized light and transparent glass for the other polarized light. This polarization selective eyepiece is referred to as see-through metasurface lens in this chapter.

To design this see-through metasurface lens, the specification of the nanorod structure shown in Fig. 4.1 should be determined. The angle of the rod of the metasurface lens is determined as shown in Eq. (4.4). In this case, the height, length, and width of the rod determine the efficiency of the metasurface lens and it is calculated through a numerical computation such as COMSOL because it is difficult to find an analytic solution. In this case, guideline for the efficiency of metasurface lens should precede the numerical computation. In case of co-polarized light which corresponds to the real-world scene, uniform transmission characteristic according to wavelength is required and maximum efficiency is needed because light intensity cannot be controlled. Meanwhile, in case of cross-polarized light that corresponds to virtual information, the light intensity is much stronger as well as the intensity can be controlled according to the wavelength, so the efficiency of co-polarized light is much important in design process. According to these guidelines, numerically designed metasurface lens have a length of 220 nm, a width of 60 nm, a thickness of 100 nm, and a unit cell pitch of 400 nm. The metasurface lens with a diameter of 20 mm is designed according to this

method and is fabricated using the nano-imprinting method. In this dissertation, the metalens is made of poly-silicon. The use of dielectrics with low thermal loss compared to other metals such as Au and Ag is advantageous in efficiency, and using silicon is advantageous because it is compatible with semiconductor CMOS processes. A scanning electron microscope (SEM) image of the actual metasurface is shown in Fig. 4.3.

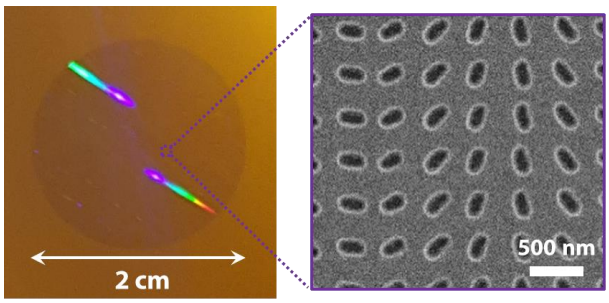

Figure 4.3 Scanning electron microscope image of metasurface. The fabrication process is conducted by Korea institute of machinery and materials (KIMM).

The fabricated metasurface lens has theoretically 79% co-polarized transmission. This is to have the most uniform efficiency for co-polarized light according to the wavelength as previously mentioned. The measured cross-polarized efficiencies are 12%, 9%, and 2.5% along the wavelength (660 nm, 532 nm, 470 nm), respectively, while the calculated efficiencies for the cross-polarized components are 29%, 6%, and 5%. The reason why the efficiency is not evenly distributed is that the optical characteristics of the material change depending on the wavelength, and in particular, in the

visible light region, the refractive index changes sharply toward blue. In addition, the structure is constant with some dimension, but it is difficult to have uniform efficiency because the coupling coefficient is dependent on the wavelength.

In the unit cell design satisfying these efficiency conditions, the metasurface lens is designed with the largest NA and use it as a near-eye display eyepiece that provides the compact and wide FOV. Therefore, the designed metasurface lens has the NA of almost 0.8, which is the limit for the sampling rate of 400 nm unit cell, so that the focal length for red, green and blue are 12.9, 16, 18 mm respectively, and these are consistent with the measurements. Since the metasurface lens modulate the phase with the geometric phase as presented in Eq. (4.4), it has different focal length depending on the wavelength. Although various studies are continuing to solve this achromatic property, there is not yet a solution that can be applied to actual application. The wavelengths of red, green and blue are 660, 532 and 473 nm, respectively. This is 0.61, 0.53, and 0.49 when converted to NA with a diameter of 20 mm, respectively, which is remarkably improved compared to IMACL with NA of 0.22.

To verify the NA and functionality of the metasurface lens, the PSF is measured using a collimated laser light as shown in Fig. 4.4. The measured PSF can be expressed to show the resolution of the system in terms of MTF. The MTF results represent the images with good resolution close to the diffraction limit can be expressed with the eyepiece.

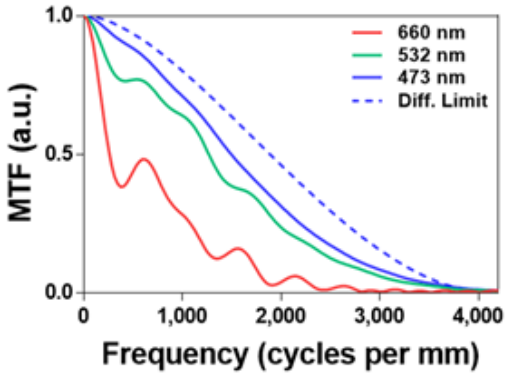

Figure 4.4 Modulation transfer function of metasurface lens.

4.3 Full-color near-eye display using metasurface lens

4.3.1 Full-color near-eye display using metasurface lens

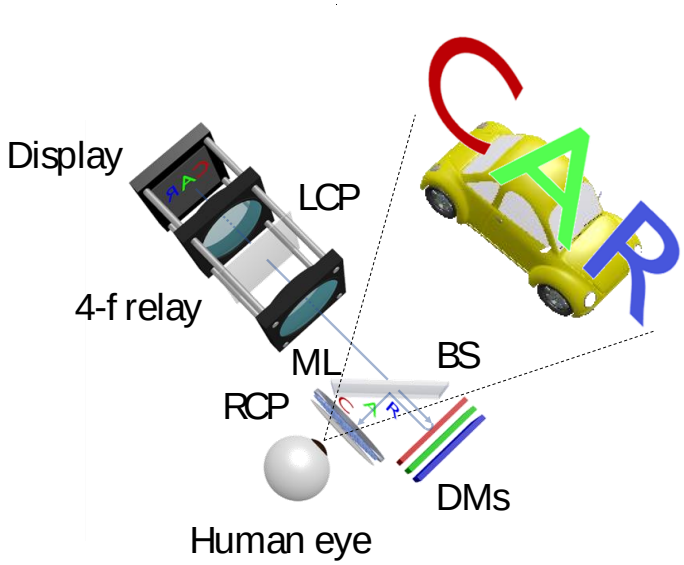

Figure 4.5 See-through near-eye display with the proposed metasurface lens.

Based on the proposed see-through metasurface lens concept, a prototype of a see-through near-eye display is designed. Figure 4.5 shows the system configuration for implementing a full-color near-eye display using the proposed metasurface. A beam projector based on the display panel with the halogen lamp is used in the prototype with natural density filter to resolve safety issue for the human eye. As described in Ch. 2, the see-through metasurface lens is located right in front of the human eye, and the image is positioned within the focal length of the metasurface lens. A beam splitter and a 4-f relay system are used to clearly demonstrate the feasibility of the proposed concept. A waveguide and a transparent screen including a diffuser holographic optical element (DHOE) are also good candidates for conveying the image to its proper position [49, 50]. For the utilization of the polarization-selective property of the metasurface lens, three polarizers exist in the system. First, a left circular polarizer is placed in front of the display. It polarizes the virtual information from the display into the left circularly polarized state. The virtual information with left circular polarization is modulated by the metasurface lens into left and right circularly polarized components. As shown in Fig. 4.2, the right circularly polarized component of the virtual information is floated to the desired depth by the metasurface lens, while the left circularly polarized component passes through the metasurface lens. The transmitted left circularly polarized component is blocked by a right circular polarizer in front of the metasurface lens, so that only the floated virtual information with right circular polarization is observed. Meanwhile, the light from the real-world scene is right circularly polarized by a right circular polarizer behind the beam splitter and enters the

metasurface lens. As shown in Fig. 4.2(c), this right circularly polarized light is modulated by the metasurface lens into a left circularly polarized component with phase modulation and a right circularly polarized component is transmitted without modulation. The right circular polarizer blocks the unnecessary left circularly polarized component of the light from the real-world scene. Ultimately, this polarization control allows the user to observe a clear image of the real-world scene that is not modulated by the metasurface lens.

Notably, as mentioned in the previous chapter, the see-through metasurface lens has different focal lengths at different wavelengths, so it cannot realize full-colour imaging with a single-layer image. Therefore, the chromatic aberration of the metasurface lens can be corrected by varying the imaging position with the wavelength using three dichroic mirrors. Figure 4.6 shows the spectra of the dichroic mirrors, the source spectrum, and Figure 4.7 shows the analysis of the effect of bandwidth on MTF.

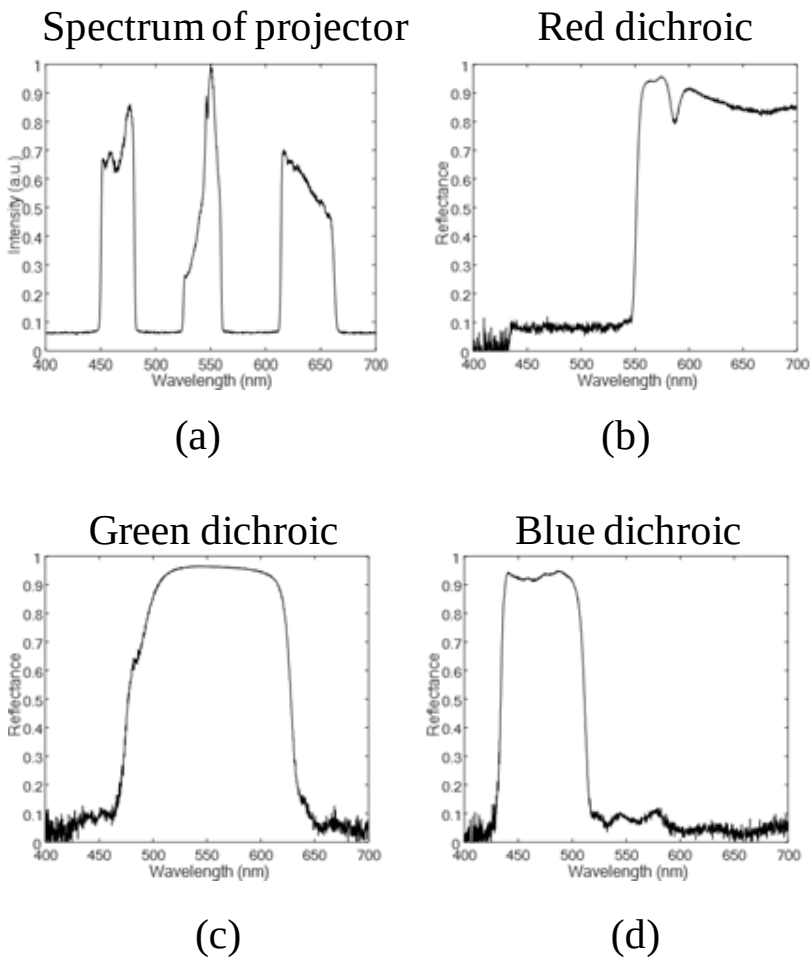

Figure 4.6 Measured spectra for (a) beam projector and (b-d) dichroic mirrors used in the experiments.

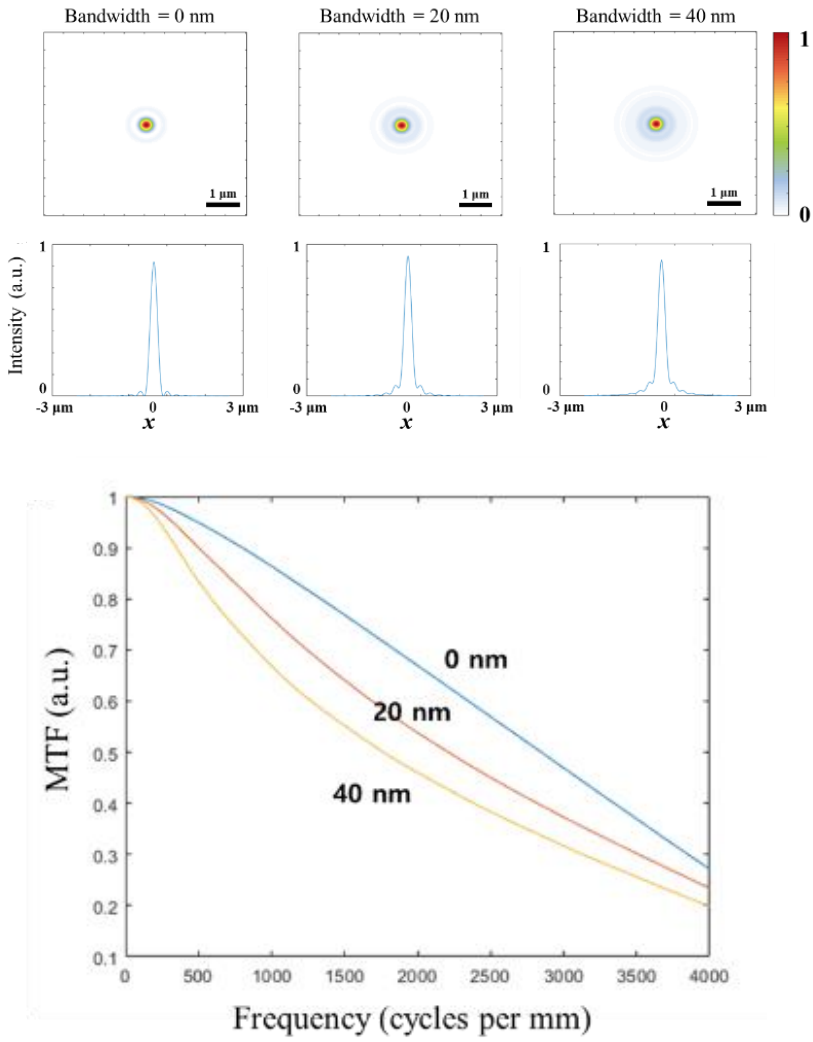

Figure 4.7 MTF analyses according to the source bandwidth.

For the metasurface whose focal length varies with wavelength, the PSF varies according to the spectrum of the input source. In the case of an input beam with a broad spectrum, sharp focus cannot be achieved because the focal length and efficiency are different. This can be analyzed as shown in

Fig. 4.7, and it can be confirmed that the MTF decreases according to the spectrum. On the actual measurement, the input spectrum is about 40 nm as shown in Fig. 4.6, which is lower than that of the ideal laser input.

This allows the system to be implemented to a full-colour see-through near-eye display system with a single display device using the metasurface lens. Although several achromatic metasurface lens have been proposed and show their possibilities, they are still not suitable for use in AR applications due to the limited sizes and NAs as well as limited anisotropy [70, 71]. In the prototype, since the desired float depth is 3 m (0.3 diopters) and the focal lengths of the metasurface lens are 12.9 mm, 16 mm and 18 mm at the target wavelengths (660 nm, 532 nm, and 473 nm, respectively), the corresponding images should be located 12.9 mm, 16 mm and 18 mm in front of the metasurface lens, respectively.

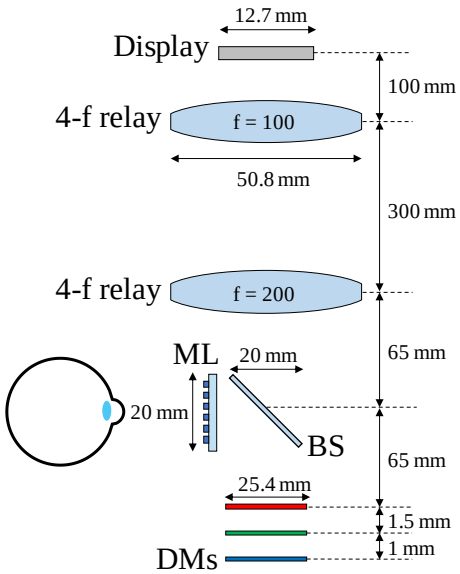

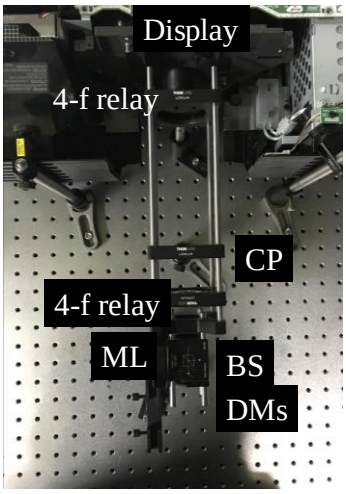

Figure 4.8 Configuration of near-eye display with metasurface lens.

Figure 4.8 shows the benchtop prototype used in the experiments. The spatial light modulator (SLM) in the Sony projector is used. To show wide FOV of the proposed see-through near-eye display, the lenses with focal length of 100 mm and 200 mm are used and magnifies the SLM of projector 2 times. The lens aperture is 20 mm and half mirror of 28 mm by 20 mm is used for beam split.

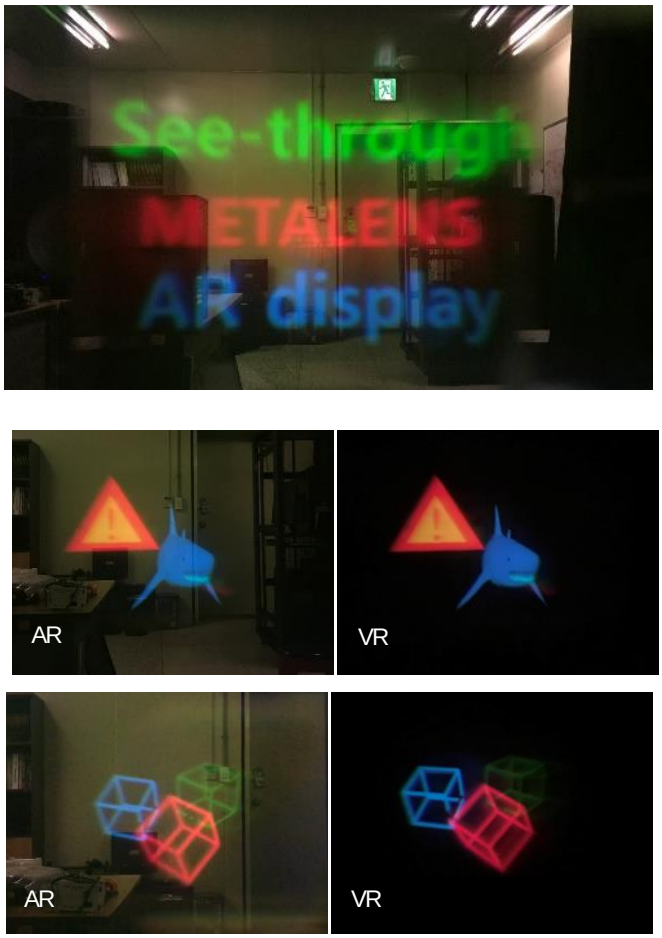

Figure 4.9 Experimental results of near-eye display with see-through metasurface lens.

Figure 4.9 shows the experimental results for full color at three wavelengths (660 nm, 532 nm, and 473 nm). Since the spherical aberration is lower than that of a conventional lens due to the nature of the metasurface lens, the image is not much distorted in the edge region despite the wide FOV. The box and shark image show the augmented images (for AR) and

the corresponding virtual images (for virtual reality). Since the efficiency of the metasurface lens varies with the wavelength, this variation is compensated on the display side. The overall efficiency of the prototype system was measured as 1 %.

The greatest advantage of using the proposed metasurface lens in a see-through near-eye display is that the eyepiece can be placed just in front of the eye, so the FOV is solely determined by the eye relief distance and the lens aperture. In the experiments, the lens aperture is 20 mm and the focal lengths are 12.9 mm, 16 mm, and 18 mm for the three wavelengths. The fixed eyebox and the eye relief of 10 mm is set to synchronize with the actual prototype specification. The prototype can have maximum FOV of 90° because the lens aperture is limited to 20 mm. The minimum display size to provide the maximum FOV depends on the focal length. In other words, the required display size differs according to the wavelength in metasurface lens. For red colour (660 nm), the 26 mm image size is required to provide the maximum FOV, while the 36 mm display size is required for a blue colour (473 nm). Therefore, the display size of 36 mm is required to provide a full colour image with the maximum FOV of 90°. However, in the prototype, the beam splitter and display with a size of 28 mm are used; Thus, it can provide an FOV of 90 ° only for red light as shown in Fig. 4.10.

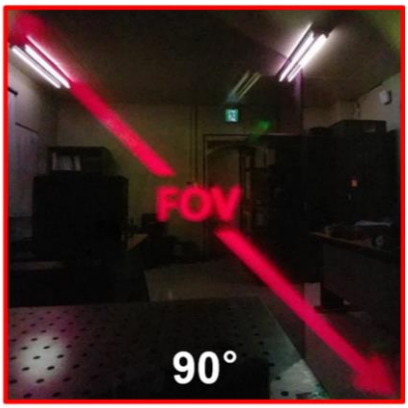

Figure 4.10 FOV verification of the proposed prototype.

For full-colour imaging, all three colours (red, green, and blue) should be represented simultaneously, and the common region in which all three colours can be displayed is the same as the blue display region, which has the narrowest FOV. Therefore, the prototype achieves an FOV of 90° for monochrome imaging and an FOV of 76° for full-colour imaging. The wide FOV of this system relative to its form factor is possible due to the novel optical properties of the metasurface lens, especially the polarization selectivity and the high NA with a large lens aperture. Consequently, the proposed system can provide a wider FOV than any other conventional near-eye display systems for AR.

Figure 4.11 shows the compact version of the proposed near-eye display system. The 4-f relay and the display are replaced more compact device such that the monochromatic compact prototype is implemented.

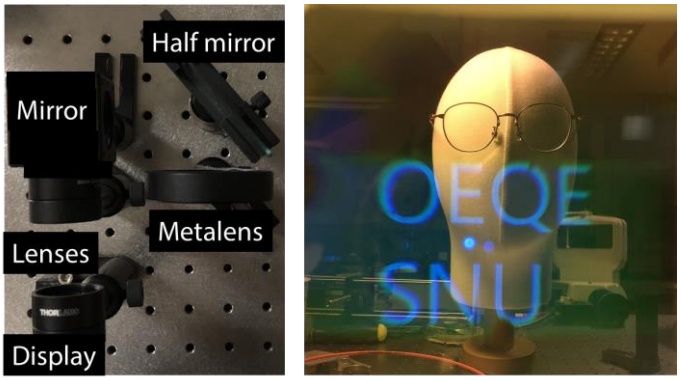

Figure 4.11 Compact near-eye display with metasurface lens.

Although the system successfully provides a wide FOV in a suitable compactness compared to other systems, the compactness of the system remains to be improved. For example, several systems using HOE have shown more compact systems, but with a very small eyebox due to the angular selectivity of the volume grating [49]. In case of the half mirror, there are several points that interfere with compactness but can be improved in the future. First, the chromatic dispersion of our metasurface lens makes the system bigger because it requires the use of three dichroic mirrors to implement the full-colour imaging. For this, the further development of an achromatic metasurface lens for AR applications could be a possible solution. As mentioned before, the current achromatic metasurface lenses are not capable of providing clear see-through property as well as large aperture with high NA due to limited control of dispersion. However, these approaches are enough to show the great potential of the achromatic metasurface lens in AR application [68, 69]. With the development of this achromatic metasurface lens for the see-through metasurface lens, the

volume of the proposed system can be mitigated. Next, a holographic method can also be a solution for this. A method of sending virtual images with different focal lengths at the display stage can be considered in the further study, and the holographic technology can make it possible to reconstruct different wavefront to compensate the different focal lengths of the metasurface lens. This method does not need the dichroic mirrors either, so this approach is one of the proper solutions for the chromatic aberration of the current see-through metasurface lens. Finally, a half mirror in the system can be improved to make the system smaller. Recent advances in metasurfaces have shown that the various works for developments of multifunctional mirrors are going on. For example, the reflection on the metasurface can be designed differently from the general reflection and the high reflection angle from the metasurface can be achieved [69]. This high reflection angle with the designed reflection relationship will make the AR system more compact owing to the reduction of the tilted angle of the half mirror.

4.3.2 Holographic near-eye display using metasurface lens for aberration compensation

The near-eye display with metasurface lens proposed in Chapter 4.3.1 has the advantage of providing wide FOV and relatively compact system. However, since the metasurface lens has single phase profile as shown in Eq. (4.4), distortion occurs including astigmatism, coma, and defocus. The distortion leads to degradation of image quality as shown in Fig. 4.12.

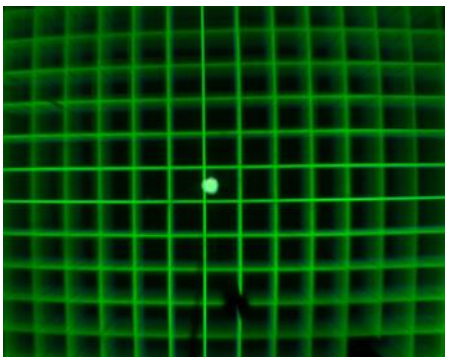

Figure 4.12 Distorted image in near-eye display with metasurface lens.

Therefore, the aberration correction can be performed using the holographic display method. The holographic display also has the advantage that the achromatic aberration can be adjusted without using the dichroic mirrors. In order to compensate for this distortion, the wavefront is pre-compensated as presented as follows:

$$U_1(\xi,\eta) = \frac{1}{r}\exp\left(-jk\sqrt{f^2+(\xi-x)^2+(\eta-y)^2}\right), \tag{4.5}$$

where, r is distance between the point and the position of the lens, k is wavenumber, x and y are position of the point light source, ξ and η are the position of lens, and f is focal length of the metasurface lens.

$U_1(\xi,\eta)$ represents a wavefront propagated from a point light source to focal length of metasurface lens. After metasurface lens, the phase of the wavefront (θ_l) is modulated as presented in Eq. (4.6).

$$\theta_l = k\left(-\sqrt{f^2+(\xi-x)^2+(\eta-y)^2}+f-\sqrt{\xi^2+\eta^2+f^2}\right). \tag{4.6}$$

The wavefront is multiplied with the phase of the metasurface lens to reproduce the parallel light. However, phase of metasurface lens leads to various aberrations such as coma, astigmatism, and defocus as shown in Eq. (4.6). To correct these aberrations, pre-compensation phase (θ_z) should be multiplied to make parallel light as presented in Eq. (4.7).

$$\theta_z = k(\sqrt{f^2 + (\xi - x)^2 + (\eta - y)^2} + \sqrt{\xi^2 + \eta^2 + f^2} + \xi \sin(\theta_x) + \eta \sin(\theta_y). \tag{4.7}$$

Using this compensation term, the wavefront to be corrected on the SLM plane can be achieved.

However, in practice, these distortion corrections do not fit precisely due to misalignment, incomplete collimation and the pixel structure of the SLM. Therefore, the actual PSF must be measured and be compensated. A Zernike polynomial is usefully adopted to modulate the wavefront during this distortion correction. The Zernike polynomial is the basis for the circular space, which is often used to represent the aberration of a lens with a circular aperture. The Zernike polynomial can express various aberrations such as defocus, astigmatism, and coma.

However, since compensating PSF at all points requires excessively huge computation load, the PSF of the sampled point is corrected and the hologram is implemented by interpolating the corresponding Zernike coefficient. The corrected points are shown in Fig. 4.13.

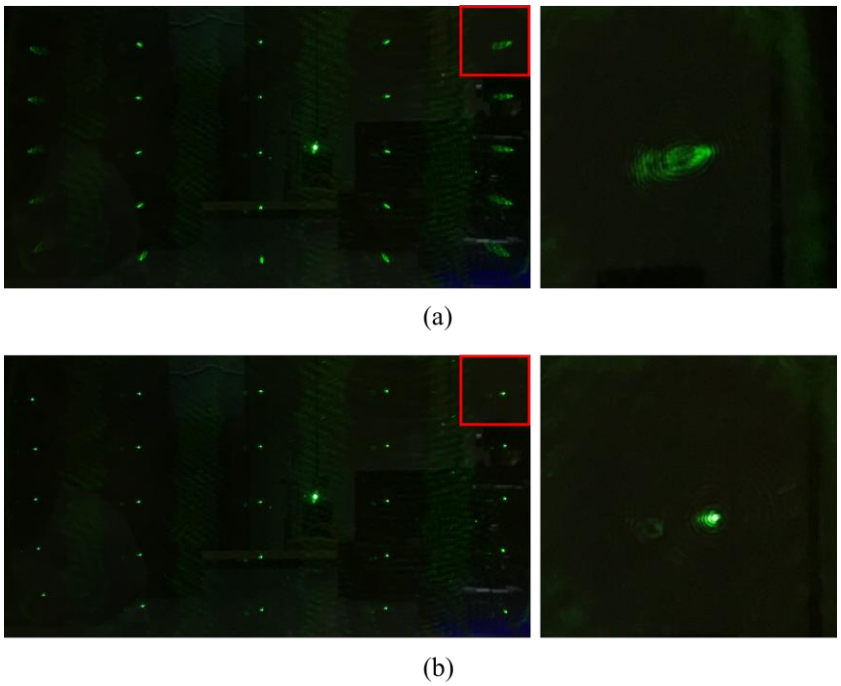

Figure 4.13 Compensation of PSF in near-eye display with metasurface lens: (a) without compensation (b) with compensation.

Figure 4.13(a) shows the PSF of the point distorted by the metasurface lens, and the coma, astigmatism and defocus appear at the edge part. As discussed earlier, by adjusting the Zernike coefficients, the PSF can be corrected as shown in Fig. 4.13(b). The Zernike coefficient map obtained by interpolating the Zernike coefficients for the 25 points obtained using this is shown in the following Fig. 4.14.

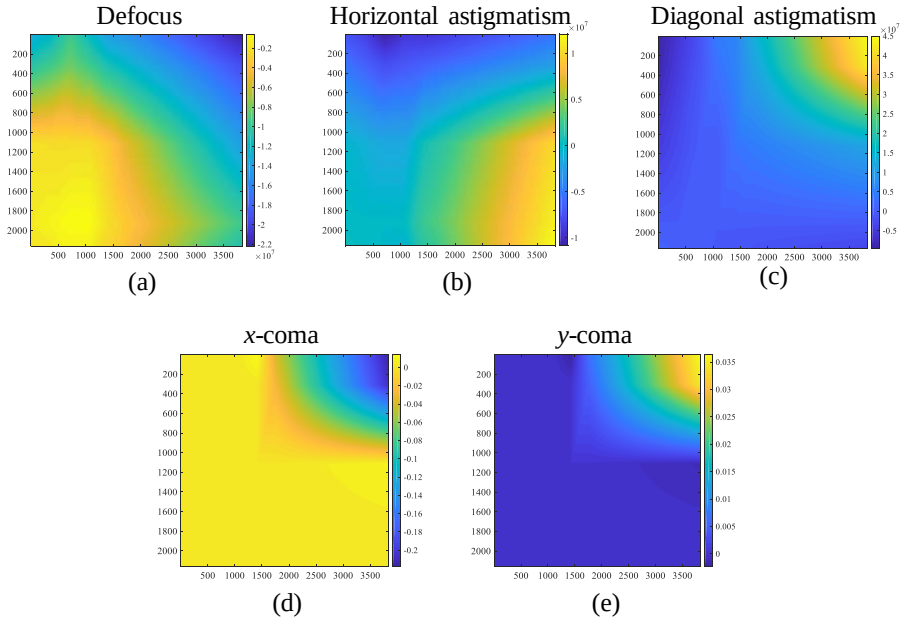

Figure 4.14 Interpolated Zernike coefficient: (a) defocus, (b) horizontal astigmatism, (c) diagonal astigmatism, (d) *x*-coma, and (e) *y*-coma.

Holographic experimental results using grid image is presented as shown in Fig. 4.15 to verify that the Zernike coefficient obtained by interpolation can compensate the aberration to the whole image

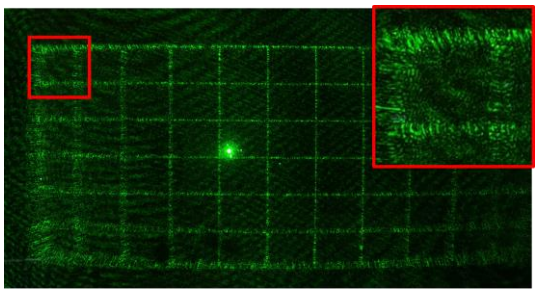

(a)

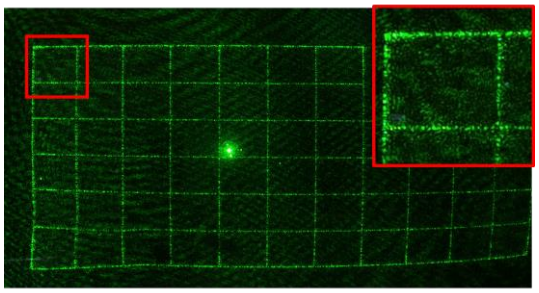

(b)

Figure 4.15 Floated hologram image with metasurface lens: (a) without wavefront compensation and (a) with wavefront compensation.

In Fig. 4.15(a), the image is not clear at the edge part without distortion correction, but as shown in Fig. 4.15(b), the distortion is corrected, and the focused grid image is obtained. The configuration and actual system of holographic near-eye display with metasurface lens implemented by using this corrected hologram are shown in Fig. 4.16.

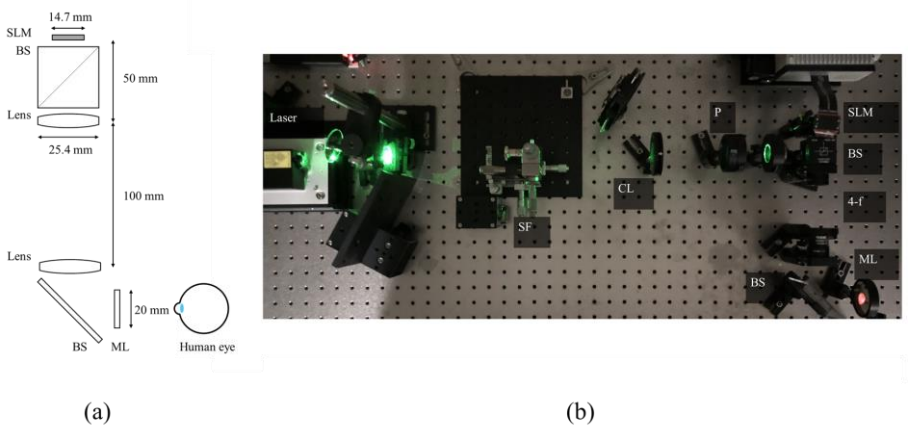

(a) (b)

Figure 4.16 Holographic near-eye display with metasurface lens (a) system configuration and (b) actual implemented system. BS is beam splitter, ML is metasurface lens, CL is collimation lens, SF is spatial filtering, and P is polarizer.

4k SLM (Jasper JD8714) is used for phase-only hologram and two 1-inch lenses whose focal length is 50 are used for 4-f relay. The green laser (532 nm) is used as collimated light. The hologram image is floated 15.9 mm in front of the metasurface lens, so the image is floated to the 2.5 m. Figure 4.17 shows the experimental results of holographic near-eye display with metasurface lens.

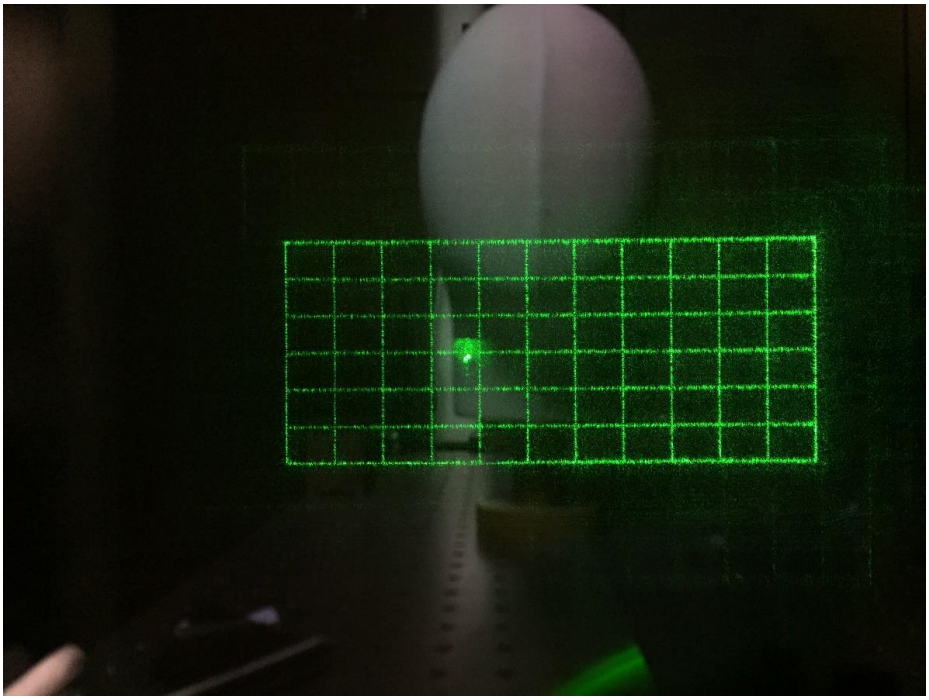

Figure 4.17 Augmented reality view with holographic near-eye display with metasurface lens.

4.4 Conclusion

In this chapter, a metasurface application has been proposed to realize a see-through near-eye display system with a wide FOV. Utilizing a sophisticatedly engineered anisotropic nanostructure, a see-through metasurface lens has been implemented that functions as transparent glass for light from real-world scenes and as an eyepiece for floating virtual information. The transmission-type eyepiece can achieve a wider FOV than is possible in previously developed systems based on conventional optics. To satisfy the criteria for AR display, the see-through metasurface lens is optimized to have

a uniform transmittance spectrum for co-polarized transmission, resulting in a clear view of the real-world scene without chromatic distortion. Via nano-imprinting technology, a prototype metasurface lens with a lens aperture of 20 mm and a high NA of 0.61 has been fabricated to demonstrate the ability to achieve a wide FOV. Consequently, a see-through augmented image with a wide FOV of 90° has been experimentally achieved in the proposed system. In addition, aberrations induced with the metasurface lens is compensated by the holographic display technique. It is expected that the combination of metasurface lens and holographic display would be a next generation near-eye display technique.

Chapter 5 Conclusion

Recently, active research on near-eye displays has been continuing to realize augmented reality due to its high sense of immersion and user-friendly interface. Among the important performances of the near-eye displays, the field of view is one of the most important optical evaluation indicators by conveying a seamless and immersive experience to the user. In this dissertation, a transmissive eyepiece has been proposed instead of a conventional reflective eyepiece. In order to realize such a transmissive eyepiece, an optical element must be developed which allows real-world scene to be transmitted, and at the same time, virtual information is floated at the desired distance.

An index-matched anisotropic crystal lens, which reacts differently depending on the polarized light, is proposed to realize this transmissive eyepiece. A refractive index anisotropic crystal lens composed of an anisotropic crystal lens and an isotropic crystal surrounding it operates differently depending on polarization. Such a transmissive eyepiece can provide a wider FOV than conventional near-field displays but has a disadvantage that the size of the system increases due to a small index difference of the anisotropic crystal.

Therefore, to realize further improvement, the metasurface is brought to the augmented reality display field. A see-through metasurface lens is proposed to realize a near-eye display with a wide FOV by using remarkable optical performance of the metasurface that surpasses conventional optical elements. The see-through metasurface lens responding differently to

polarized light can realize a wide FOV and relatively compact system.

Although a lot of advantages, the researches on the proposed transmissive eyepiece system is still many challenges to solve. Especially, in terms of form factor, the near-eye display using DOE and waveguide shows the possibility to realize extremely thin form factor. On the contrary, the near-eye display using transmissive eyepiece described in this dissertation is limited to the bird bath system. In addition, the achromatic aberration of see-through metasurface lens requires additional optical (dichroic mirrors) which induces bulky form factor. In order to mitigate the disadvantages on the form factor, the preliminary method using a holographic display has been proposed at the end of the dissertation. However, in order to take a wide FOV and a compact form factor at the same time, a new approach such as achromatic metasurface lens or combination of waveguide and metasurface lens, should be studied.

Bibliography

1. P. Milgram, H. Takemura, A. Utsumi, F. Kishino. “Augmented Reality: A class of displays on the reality-virtuality continuum” Proceedings of Telemanipulator and Telepresence Technologies. 2351–34(1994).
2. R. T. Azuma, “A survey of augmented reality,” Presence: Teleoperators and virtual environments, vol. 6, no. 4, 335-385(1997).
3. C. Wheatstone “I. The Bakerian Lecture.—Contributions to the physiology of vision.—Part the second. On some remarkable, and hitherto unobserved, phenomena of binocular vision (continued).” Philosophical transactions of the Royal Society of London, vol. 142, 1-17(1852).
4. E. Deville, “On the use of the Wheatstone stereoscope in photographic surveying,” Transactions of the Royal Society of Canada, vol. 8, 63-69(1902).
5. J. P. McIntire, P. R. Havig and E. E. Geiselman, “Stereoscopic 3D displays and human performance: A comprehensive review,” Displays, vol. 35, no. 1, 18-26 (2014).
6. I. Sexton, and P. Surman, “Stereoscopic and autostereoscopic display systems,” IEEE Signal Processing Magazine, vol. 16, no. 3, 85-99(1999).
7. N. A. Dodgson, “Autostereoscopic 3D displays,” Computer, vol. 8, 31-36(2005).
8. W. Matusik, and H. Pfister, “3D TV: a scalable system for real-time acquisition, transmission, and autostereoscopic display of dynamic scenes,” In ACM Transactions on Graphics (TOG) vol. 23, no. 3, 814-

824(2004).

9. J. Hong, Y. Kim, H.-J. Choi, J. Hahn, J.-H. Park, H. Kim, S.-W. Min, N. Chen, and B. Lee, “Three-dimensional display technologies of recent interest: principles, status, and issues,” Applied Optics, vol. 50, no. 34, H87-H115(2011).
10. I. E. Sutherland, “A head-mounted three dimensional display.” Proceedings of the December, 9-11(1968).
11. B. Kress, and S. Thad, “A review of head-mounted displays (HMD) technologies and applications for consumer electronics,” Proc. SPIE. vol. 8720(2013).
12. W. Robinett, and J. P. Rolland, “A computational model for the stereoscopic optics of a head-mounted display,” Presence: Teleoperators & Virtual Environments, vol. 1, no. 1, 45-62(1992).
13. J.-H. Park, K. Hong, and B. Lee, “Recent progress in three-dimensional information processing based on integral imaging,” Applied Optics, vol. 48, no. 34, H77-H94(2009).
14. R. W. Gubisch, “Optical performance of the human eye.” JOSA, vol. 57, no. 3, 407-415(1967).
15. B. Guenter, M. Finch, S. Drucker, D. Tan, and J. Snyder, “Foveated 3D graphics,” ACM Transactions on Graphics (TOG), vol. 31 no. 6, 164(2012).
16. A. Patney, J. Kim, M, Salvi, A. Kaplanyan, C. Wyman, N. Benty, and D. Luebke, “Perceptually-based foveated virtual reality,” In ACM SIGGRAPH 2016 Emerging Technologies, 17(2016).
17. G. Dagnelie, “Visual prosthetics: physiology, bioengineering,

rehabilitation," Springer Science & Business Media (2011).

18. E. M. Howlett, "High-resolution inserts in wide-angle head-mounted stereoscopic displays," In Stereoscopic Displays and Applications III International Society for Optics and Photonics, vol. 1669, 193-204(1992).
19. S. Liu, H. Hua, "A systematic method for designing depth-fused multi-focal plane three-dimensional displays," Optics express, vol. 18, no. 11, 11562-11573(2010).
20. D. M. Hoffman, A. R. Girshick, K. Akeley, and M. S. Banks, "Vergence–accommodation conflicts hinder visual performance and cause visual fatigue," Journal of vision, vol. 8, no. 3, 33-33(2008).
21. T. Bando, A. Iijima, and S. Yano, "Visual fatigue caused by stereoscopic images and the search for the requirement to prevent them: A review," Displays, vol. 33, no. 2, 76-83(2012).
22. Microsoft, Co., Microsoft HoloLens. https://www.microsoft.com/microsoft-hololens/en-us (Date of access: 06/04/2017) (2014).
23. C. Jang, K. Bang, S. Moon, J. Kim, S. Lee, and B. Lee, "Retinal 3D: augmented reality near-eye display via pupil-tracked light field projection on retina," ACM Transactions on Graphics, vol. 36, no. 6, 190(2017).
24. Oculus VR, LLC., Oculus rift. https://www.oculus.com/rift/ (Date of access:06/04/2017) (2015).
25. Samsung Electronics, Ltd., Samsung Gear VR. http://www.samsung.com/global/galaxy/gear-vr/ (Date of access: 06/04/2017) (2015).

26. Meta Vision, Co., Meta Vision. http://www.metavision.com (Date of access: 06/04/2017) (2015).
27. Google, Co., Glass, https://x.company/glass/ (Date of access: 30/10/2018) (2017).
28. S. Moon, C.-K. Lee, D. Lee, C. Jang, and B. Lee, “Layered display with accommodation cue using scattering polarizer,” IEEE Journal of Selected Optics in Signal Processing, vol. 11, no. 7, 1223-1231 (2017).
29. D. Cheng, Y. Wang, H. Hua, and M. M. Talha, “Design of an optical see-through head-mounted display with a low f-number and large field of view using a freeform prism,” Applied optics, vol. 48, no. 14, 2655-2668(2009).
30. D. Cheng, Y. Wang, H. Hua, and J. Sasian, “Design of a wide-angle, lightweight head-mounted display using free-form optics tiling,” Optics letters, vol. 36, no. 11, 2098-2100(2011).
31. T. Levola, “Diffractive optics for virtual reality displays,” Journal of the Society for Information Display, vol. 14, 467-475(2006).
32. T. Levola, “7.1: Invited paper: Novel diffractive optical components for near to eye displays,” In SID Symposium Digest of Technical Papers, vol. 37, 64-67(2006).
33. A. Maimone, A. Georgiou, and J. S. Kollin, “Holographic near-eye displays for virtual and augmented reality,” ACM Transactions on Graphics, vol. 36 85(2017).
34. S. Lee, B. Lee, J. Cho, C. Jang, J. Kim, and B. Lee, “Analysis and implementation of hologram lenses for see-through head-mounted display,” IEEE Photonics Technology Letters, vol. 29, no. 1, 82-

85(2017).

35. I. Kasai, Y. Tanijiri, E. Takeshi, and U. Hiroaki, “A practical see-through head mounted display using a holographic optical element,” Optical review, vol. 8, 241-244(2001).
36. S.-g. Park, J. Yeom, Y. Jeong, N. Chen, J.-Y. Hong, and B. Lee, “Recent issues on integral imaging and its applications,” Journal of Information Display, vol. 15, no. 1, 37-46(2014).
37. Y. Kim, K. Hong, and B. Lee, “Recent researches based on integral imaging display method,” 3D Research, vol. 1, no. 1, 17-27(2010).
38. S. Suyama, S. Ohtsuka, H. Takada, K. Uehira, and S. Sakai, “Apparent 3-D image perceived from luminancemodulated two 2-D images displayed at different depths,” Vision Res., vol. 44, no. 8, 785-793 (2004).
39. S.-g. Park, J.-H. Jung, Y. Jeong, and B. Lee, "Depth-fused display with improved viewing characteristics," Optics Express, vol. 21, no. 23, pp. 28758-28770, 2013.
40. K. Akeley, S. J. Watt, A. R. Girshick, and M. S. Banks, “A stereo display prototype with multiple focal distances” ACM Trans. Graph. (SIGGRAPH), vol. 23, 804–813(2004).
41. R. Narain, R. A. Albert, A. Bulbul, G. J. Ward, M. S. Banks, and J. F. O'Brien, “Optimal presentation of imagery with focus cues on multi-plane displays,” ACM Transactions on Graphics (TOG), vol. 34, no. 4, 59(2015).
42. C.-K. Lee, S.-g. Park, S. Moon and B. Lee, “Viewing zone duplication of multi-projection 3d display system using uniaxial crystal,” Optics

express, vol. 24, 8458-8470(2016).

43. G. D. Love, D. M. Hoffman, P. J. Hands, J. Gao, A. K. Kirby and M. S. Banks, “High-speed switchable lens enables the development of a volumetric stereoscopic display,” Optics express, vol. 17, no. 18, 15716-15725(2009).
44. C.-K. Park, S.-S. Lee, and Y.-S. Hwang, “Depth-extended integral imaging system based on a birefringence lens array providing polarization switchable focal lengths,” Optics express, vol. 17, 19047–19054(2009).
45. N. Nieuborg, A. Kirk, B. Morlion, H. Thienpont and I. Veretennicoff, “Polarization-selective diffractive optical elements with an index-matching gap material,” Applied optics, vol. 36, 4681–4685(1997).
46. J. P. Lesso, A. J. Duncan, W. Sibbett and M. J. Padgett, “Aberrations introduced by a lens made from a birefringent material,” Applied optics, vol. 39, 592-598(2000).
47. G. Gajdátsy and M. Erdélyi, “Analysis of focus distortion based on birefringence,” Journal of Optics A: Pure and Applied Optics, vol. 9, 982 (2007).
48. Optical solutions. CODE V: Optical Design Software. Synopsys, Pasadena, California URL https://optics.synopsys.com/codev/.
49. J. Yeom, J. Jeong, C. Jang, K. Hong, S.-g. Park, and B. Lee, “Reflection-type integral imaging system using a diffuser holographic optical element,” Optics Express, vol. 22, no. 24, 29617-29626(2014).
50. J. Yeom, J. Jeong, C. Jang, G. Li, K. Hong, and B. Lee, “Three-dimensional/two-dimensional convertible projection screen using see-

through integral imaging based on holographic optical element," Applied Optics, vol. 54, no. 30, 8856-8862(2015).

51. J.-Y. Hong, S.-g. Park, C.-K. Lee, S. Moon, S.-J. Kim, J. Hong, Y. Kim, and B. Lee, "See-through multi-projection three-dimensional display using transparent anisotropic diffuser," Optics Express, vol. 24, no. 13, 14138-14151, (2016).
52. J. Hong, Y. Kim, S.-G. Park, J.-H. Hong, S.-W. Min, S.-D. Lee, and B. Lee, "3D/2D convertible projection-type integral imaging using concave half mirror array," Optics Express, vol. 18, no. 20, 20628-20637, (2010).
53. A. Maimone, D. Lanman, L. Rathinavel, K. Keller, D. Luebke, and H. Fuchs, "Pinlight displays: wide field of view augmented reality eyeglasses using defocused point light sources," In ACM SIGGRAPH 2014 Emerging Technologies, 20(2014).
54. S. Wadle and R. S. Lakes, "Holographic diffusers: polarization effects," Optical Engineering, vol. 33, no. 4, 1084-1089(1994).
55. N. Meinzer, N, W. L. Barnes and I. R. Hooper, "Plasmonic meta-atoms and metasurfaces," Nature Photonics, vol.8, 889–898(2014).
56. N. Yu and F. Capasso, "Flat optics with designer metasurfaces," Nature Materials, vol. 13, 139-150(2014).
57. A. I. Kuznetsov, A. E. Miroshnichenko, M. L. Brongersma, Y. S. Kivshar and B. Luk'yanchuk, "Optically resonant dielectric nanostructures," Science, vol. 354, aag2472(2016).
58. S. Jahani and Z. Jacob, "All-dielectric metamaterials," Nature Nanotechnology, vol. 11, 23-36(2016).
59. V. M. Shalaev, "Optical negative-index metamaterials," Nature Photonics, vol. 1, 41-48(2007).
60. A. Arbabi, Y. Horie, A. J. Ball, M. Bagheri and A. Faraon,

"Subwavelength-thick lenses with high numerical apertures and large efficiency based on high-contrast transmitarrays," Nature Communications, vol. 6, 7069(2015).

61. L. Huang, X. Chen, H. Mühlenbernd, H. Zhang, S. Chen, B. Bai, Q. Tan, G. Jin, K.-W. Cheah, C.-W., Qiu, J. Li, T. Zentgraf and S. Zhang, "Three-dimensional optical holography using a plasmonic metasurface," Nature Communications, vol. 4, 2808(2013).
62. G.-Y. Lee, G. Yoon, S.-Y. Lee, H. Yun, J. Cho, K. Lee, H. Kim, J. Rho and B. Lee, "Complete amplitude and phase control of light using broadband holographic metasurface," Nanoscale, vol. 10, 4237-4245 (2018).
63. J. Park, J.-H. Kang, S. J. Kim, X. Liu and M. L. Brongersma, "Dynamic reflection phase and polarization control in metasurfaces," Nano Letter vol. 17, 407–413(2017).
64. M. Wuttig, H. Bhaskaran, T. Taubner, "Phase-change materials for non-volatile photonic applications," Nature Photonics, vol. 11, 465–476 (2017).
65. M. Khorasaninejad, W. T. Chen, J. Oh and F. Capasso, "Super-dispersive off-axis meta-lenses for compact high resolution spectroscopy," Nano Letter, vol. 16, 3732–3737(2016).
66. A. Arbabi, E. Arbabi, Y. Horie, S. N. Karmali and A. Faraon, "Planar metasurface retroreflector," Nature Photonics, vol. 11, 415–420(2017).
67. A. Arbabi, Y. Horie, A. J. Ball, M. Bagheri and A. Faraon, "Subwavelength-thick lenses with high numerical apertures and large efficiency based on high-contrast transmitarrays," Nature Communications, vol. 6, 7069(2015).
68. A. Arbabi, Y. Hoie, M. Bagheri and A. Faraon, "Dielectric metasurfaces for complete control of phase and polarization with subwavelength spatial resolution and high transmission," Nature Nanotechnology, vol. 10, 937–943(2015).

69. D. Lin, P. Fan, E. Hasman, and M. L. Brongersma, “Dielectric gradient metasurface optical elements,” Science, vol. 345, 298-302(2014).
70. W. Chen, A. Y. Zhu, V. Sanjeev, M. Khorasaninejad, Z. Shi, E. Lee and F. Capasso, “A broadband achromatic metasurface lens for focusing and imaging in the visible,” Nature Nanotechnology, vol. 13, no. 3, 220(2018).
71. S. Wang, P. C. Wu, V.-C. Su, Y.-C. Lai, M.-K. Chen, H. Y. Kuo, B. H. Chen, Y. H. Chen, T.-T. Huang, J.-H. Wang, R.-M. Lin, C.-H. Kuan, T. Li, Z. Wang, S. Zhu and D. P. Tsai, “A broadband achromatic metasurface lens in the visible,” Nature Nanotechnolgy, vol. 13, no. 3, 227(2018).
72. M. Khorasaninejad, W.T. Chen, R. C. Devlin, J. Oh, A. Zhu and F. Capasso, “Metasurface lenses at visible wavelengths: Diffraction-limited focusing and subwavelength resolution imaging,” Science, vol. 352, 1190(2016).

Appendix

Portions of the work discussed in this dissertation were also presented in the following publications:

[Chapter 3] J.-Y. Hong, C.-K. Lee, S. Lee, B. Lee, D. Yoo, C. Jang, J. Kim, J. Jeong, and B. Lee, “See-through optical combiner for augmented reality head-mounted display: index-matched anisotropic crystal lens,” Scientific Reports, vol. 7, article 2753(2017).

[Chapter 4] G.-Y. Lee†, J.-Y. Hong†, S. Hwang, S. Moon, H. Kang, S. Jeong, H. Kim, J.-H. Jeong, and B. Lee, “Metasurface eyepiece for augmented

reality," Nature Communications, vol. 9, article 4562, 2018

초 록

근안 디스플레이는 높은 몰입감과 사용자 친화적인 인터페이스로 인해 증강 현실을 구현하는 가장 효과적인 기술로 최근 활발한 연구가 계속되고 있다. 이러한 근안 디스플레이의 중요한 성능 중 시야각은 매끄럽고 몰입감 있는 경험을 사용자에게 전해줌으로써 가장 중요한 광학적 평가지표 중에 하나이다. 본 논문에서는 기존의 반사형 아이피스 (eyepiece) 를 대신하는 투과형 아이피스를 제안한다. 이러한 투과형 아이피스를 구현하기 위해서는 외부 정보에 대해서는 투명한 유리와 같이 투과시키며, 동시에 가상 정보는 렌즈로 작동하여 먼 거리에 띄울 수 있는 광학소자를 개발하여야 한다.

이러한 투과형 아이피스를 구현하기 위해서 편광에 따라 다르게 반응하는 굴절률 정합 이방성 결정 렌즈 (index-matched anisotropic crystal lens) 를 제안하였다. 이방성 결정 구조 (anisotropic crystal)로 이루어진 렌즈와 이를 둘러싼 등방성 물질 (isotropic crytal) 로 이루어진 굴절률 정합 이방성 결정 렌즈는 편광에 따라 다르게 작동한다. 이러한 투과형 아이피스는 기존의 근안 디스플레이에 비해 넓은 시야각을 제공할 수 있지만 이방성 결정 구조의 낮은 굴절률 차이로 인해 시스템의 크기가 커지는 단점을 가지고 있다.

본 논문에서는 이러한 단점을 개선하기 위해 메타 표면을 증강현실 디스플레이 분야에 적용하였다. 메타 표면의 기존 광학 소자를 능가하는 놀라운 광학 성능을 이용하여 넓은 시야각을 가지는 근안 디스플레이를 구현하기 위해 투명 메타 렌즈를 제안하였다.

편광에 따라 다르게 반응하는 투명 메타렌즈는 넓은 시야각과 경량화 시스템 구현이 가능하며 이를 입증하기 위해 투명 메타렌즈의 설계 방법 뿐 아니라 실제 구현을 통한 가능성을 입증하였다.

이러한 새로운 아이피스에 대한 개념은 기존의 근안 디스플레이의 사양 개선에 유용하게 사용될 뿐 아니라 차세대 근안 디스플레이를 위한 선도적인 역할을 할 것으로 기대된다.

주요어: 증강현실 디스플레이, 메타표면, 메타표면 렌즈, 비등방성 결정 물질, 굴절률 정합, 홀로그래픽 광학 소자

학번: 2013-20910